01 Nov 1965

Torsional-flexural buckling of thin-walled open sections

Pen J. Fang

George Winter

CCFSS LIBRARY Fang, Pen J. Winter, George
22 1 * 109 TORSIONAL-FLEXURAL BUCKLING OF
c2 THIN-WALLED OPEN SECTIONS

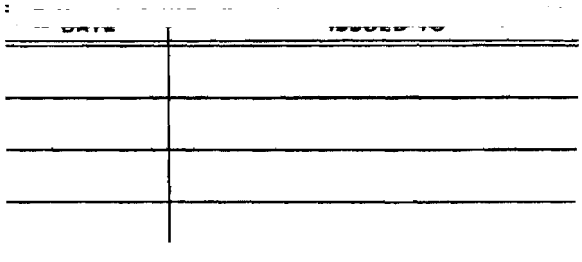

Department of Structural Engineering
School of Civil Engineering
Cornell University

Report No. 320A

TORSIONAL-FLEXURAL BUCKLING OF THIN-WALLED OPEN SECTIONS

by

Pen J. Fang
Research Assistant

George Winter
Project Director

A research project sponsored by the
American Iron and Steel Institute

Ithaca, New York November, 1965

CONTENTS

INTRODUCTION

Compression members with thin-walled open sections, because of their low torsional rigidities and because their cross-sectional configuration is such that the centroid and the shear center often do not coincide, can buckle at loads well below the Euler load by interaction of torsion and bending. Fast expanding applications of such sections in civil and architectural engineering call for an extensive investigation of torsional-flexural buckling.

Basic theory of torsional-flexural buckling is treated by a number of authors,[1,2] and simplifications of the basic theory in the elastic range for the design purposes together with some test results were reported previously.[3] Some investigation of inelastic torsional-flexural buckling of as-rolled, thick-walled I-beams by application of bi-axial moments has been reported.[6,7,8] However, there has not been sufficient investigation of axially loaded columns with thin-walled open sections in the inelastic range.

All inelastic buckling problems are inherently non-linear and non-static. In view of the even more complex nature of torsional-flexural buckling, simplifications of the basic theory for practical purposes are necessary. While the simplification may reduce the design procedure to an easier form, the computed values must also be reasonably accurate when compared to the actual buckling loads.

This investigation, primarily semi-empirical, was conducted for the following objectives:

1. To develop and verify an approximate inelastic torsional-flexural buckling theory based on certain simplifying assumptions.

2. To recommend a practical design procedure and a formulation of code provisions against torsional-flexural buckling covering both the elastic and inelastic ranges.

A series of tests on specimens of various cross-sectional shapes and dimensions was made to verify the basic theory. The test results agree with the predicted values within reasonable limits.

BASIC THEORY

Axially compressed members with thin-walled open sections, because of their low torsional rigidities, can buckle by twisting at loads well below the Euler load. Also, because of their cross-sectional configuration, the centroid and the shear center frequently do not coincide and, therefore, torsion and flexure interact.

Members having singly symmetrical cross-sections may buckle in pure flexure or in the torsional-flexural mode. Based on linear theory,[1,2,3] the critical torsional-flexural stress in the elastic range is given by the following quadratic interaction equation:

$$(\sigma_{cr})_E = \frac{1}{2K}\left[(\sigma_x + \sigma_\phi) - \sqrt{(\sigma_x + \sigma_\phi)^2 - 4K\,\sigma_x\,\sigma_\phi}\,\right] \quad (1a)$$

in which

$(\sigma_{cr})_E$ = the elastic torsional-flexural buckling stress;

$$K = 1 - \left(\frac{x_o}{r_o}\right)^2 \tag{1b}$$

$$\sigma_x = \frac{\pi^2 E}{(L/r_x)^2} \tag{1c}$$

$$\sigma_\phi = \frac{1}{I_p}\left[GJ + \frac{E\,C_w \pi^2}{L^2}\right] \tag{1d}$$

x_o = the coordinate of the shear center with regard to the centroid;

r_o = the polar radius of gyration about the shear center

$$= \sqrt{\frac{I_x + I_y}{A} + x_o^2} \quad ;$$

r_x = the radius of gyration about the x-axis;

A = the cross-sectional area;

I_p = the polar moment of inertia about the shear center.

For thin-walled open sections comprised of plate elements which do not significantly restrain each other torsionally, Eq. (1a) gives a rather accurate account of the interaction of the two fundamental modes.

For members of small or moderate slenderness with walls of greater thicknesses, the average compressive stress prior to buckling may exceed the proportional limit of the material. In this case failure occurs at an inelastic torsional-flexural stress which is less than the computed elastic buckling stress.

According to the tangent modulus theory, the flexural buckling stress in the inelastic range (buckling about the

x-axis) is given by the well-known Engesser-Shanley equation:

$$(\sigma_x)_t = \frac{\pi^2 E_t}{(L/r_x)^2} \qquad (2)$$

In the analysis and derivation of the equations governing torsional-flexural buckling in the elastic range, the so-called Euler method is used.[1,3] Many practical column problems including torsional-flexural buckling in the elastic range can be treated as static buckling problems for perfect mathematical models. A static stability criterion may not be useful, however, for nonlinear problems. Shanley pointed out that the time factor and behavior of loading must be taken into account in the inelastic column buckling, which leads to the tangent modulus concept, in contrast to the double modulus theory of v. Karman which is the result of a mere extension of the Euler method.

The critical average compression stress of the purely torsional mode in the inelastic range is then

$$(\sigma_\phi)_t = \frac{1}{I_p}\left[G_t J + \frac{E_t C_w \pi^2}{L^2}\right] \qquad (3)$$

in which E_t is the tangent modulus defined by $\frac{d\sigma}{d\varepsilon}$, and G_t = the tangent modulus of shear defined by $\frac{d\tau}{d\sigma}$. Eq. (3) comes directly from Eq. (1d) because during buckling in the inelastic range, infinitesimal shear stresses $d\tau$ are superimposed on axial compressive stresses, the ratio between excess shear stresses and excess shear strain being G_t. The second term in the bracket of Eq. (1d) represents the component of internal resisting torque due to warping of the column

as it twists, E refers to the axial stress thus caused; hence in the inelastic range, it becomes E_t by applying the Shanley inelastic buckling concept.

Thus,the critical torsional-flexural buckling stress in the inelastic domain can be given by

$$(\sigma_{cr})_t = \frac{1}{2K}\left[(\sigma_x)_t + (\sigma_\phi)_t - \sqrt{\{(\sigma_x)_t+(\sigma_\phi)_t\}^2 - 4K(\sigma_x)_t\,(\sigma_\phi)_t}\right] \quad (4)$$

There are several theories and suggestions for computing the inelastic moduli in Eq. (4). However, most of the theories and methods lead to quite complicated and inconvenient procedures. For example, P. P. Bijlaard[10] derived the following expression for G_t:

$$G_t = E/(2 + 2\nu + 3e) \quad (5)$$

in which

ν = Poisson's ratio;

$e = (E/E_s) - 1$;

E_s = the secant modulus.

F. Bleich[2] suggested the relationship

$$G_t = G\sqrt{\frac{E_t}{E}} \quad (6)$$

If these expressions are substituted in Eqs. (3) and (4) and combined with an appropriate expression for the stress-strain relationship of the material, the resulting equation needs laborious and time-consuming solution. (See Appendix D.)

We shall assume now that the ratio of tangent modulus of shear to elastic modulus is equal to that of tangent

modulus to Young's modulus; namely, E_t/E, so that

$$G_t = G \frac{E_t}{E} = \frac{E_t}{2(1 + \nu)} \tag{7}$$

This is equivalent to saying that the ratio of the two moduli remains constant. This assumption is in accordance with that made by K. Roik[9] and F. Bleich[2]. It cannot be proved rigorously but may be justified qualitatively because for most cases of torsional buckling, the shearing stresses play only a minor role (although the case of the equal legged angle seems to deviate somewhat from this reasoning). Hence, even relatively crude approximations in the shear terms have comparatively little effect on computed critical loads.

The relation (7) leads to a somewhat smaller value of G_t than other expressions, and therefore, to a more conservative buckling stress. The computation is greatly simplified, however, by this approximation. Eq. (3) can then be written as

$$(\sigma_\phi)_t = \frac{1}{I_p} \left[G_t J + \frac{E_t C_w \pi^2}{L^2}\right]$$

$$= \frac{1}{I_p} \left[\frac{E_t}{2(1+\nu)} J + \frac{E_t C_w \pi^2}{L^2}\right] \tag{8}$$

In order to determine stress-strain curves of the columns, stub column tests were made. Typical effective over-all stress-strain relationship of the specimens are shown in Figs. 2, 3, 4 and 5.

All stress-strain curves reflect the well-known effects of cold forming[5]. They are practically linear up to at least half of the yield strength determined as the stress corresponding to 0.2% residual strain. Above the proportional limit,

they gradually deviate from linearity and rapidly curve as the stress approaches yielding. In the present case, the non-linearity above the proportional limit is due to the effect of cold forming which produces zones of higher yield strength at corners.

To obtain the stress-strain relationship, we assume that the E_t/E ratio follows a parabolic law; thus, the expression for E_t can be written as

$$E_t = CE \left[\frac{\sigma}{\sigma_y} - \left(\frac{\sigma}{\sigma_y}\right)^2\right] \qquad (9)$$

where

$$C = f(\sigma, \sigma_p, \sigma_y)$$

Hence, C is a numerical parameter, dependent on the full section proportional limit which in turn is dependent on the properties of virgin material, amount of cold forming and on the cross-sectional dimensions. Thus, if one has an expression for E_t as a function of stress, for given E, proportional limit and yield strength of the material, the inelastic torsional-flexural buckling can be easily calculated.

From the stress-strain curves of the stub column tests, E_t was measured using a "tangentiometer". A tangentiometer is a semi-transparent mirror fixed perpendicularly to a straight base. Holding the mirror perpendicular to the paper on which the stress-strain curve is drawn, one can adjust the position of the mirror until the reflected image of the curve coincides with the curve seen through the mirror;

the surface of the mirror is then normal to the curve at that point. The slope of the curve at the point can be read at the base. The E_t/E ratios are plotted against $\frac{\sigma}{\sigma_y}$ as shown in Fig. 6. If a curve is drawn through the center of the scatter band, C is seen to be 4.5. For comparison, a curve based on C = 4 is also plotted, and seen to represent the lower limit of the scatter band. This value, C = 4, is the one currently used for steel column design for flexural buckling, taking the proportional limit as one-half of the yield strength.

For most practical cases, the majority of buckling stresses fall under 90% of the yielding strength. It is seen from Fig. 6 that the curve corresponding to C = 4 is the lower bound of the group of the experimental data. For a more gradually yielding stress-strain curve, C tends to be lower, as is the cases of hat and lipped angle sections, Figs. (4) and (5). Conversely, C tends to be higher for angle section, Fig. (2), while for channel section it is about the intermediate, Fig. (4). This effect can be observed later from the buckling test results plotted in Fig. (14). The points for hat and lipped angle sections generally fell somewhat below the theoretical curved based on C = 4.5 and those for angle section are generally above the curve, with those for channel section being in best agreement with the theoretical curve.

The tangent modulus can then be expressed as

$$E_t = 4.5\ E\ [\frac{\sigma}{\sigma_y}\ (1 - \frac{\sigma}{\sigma_y})] \qquad (10)$$

To derive a stress-strain curve from this equation, one notes that

$$E_t = \frac{d\sigma}{d\epsilon}$$

and substitutes this differential into Eq. (10) to get

$$\epsilon = \frac{1}{4.5E} \int \frac{d\sigma}{\frac{\sigma}{\sigma_y}(1 - \frac{\sigma}{\sigma_y})}$$

carrying out the integration

$$\epsilon = C_1 + \frac{1}{4.5E} \ln \left| \frac{\sigma/\sigma_y}{1 - \sigma/\sigma_y} \right|$$

The constant of integration, C_1, can be determined by the condition of the proportional limit, i.e.,

$$\frac{E_t}{E}\Big|_{\sigma_p} = 1$$

whence, Eq. (10) becomes

$$1 = 4.5 \left[\frac{\sigma_p}{\sigma_y} - \left(\frac{\sigma_p}{\sigma_y}\right)^2\right]$$

Solving for $\frac{\sigma_p}{\sigma_y}$, one obtains

$$\frac{\sigma_p}{\sigma_y} = \frac{2}{3}$$

thus the proportional σ_p above which Eq. (10) applies, is

$$\sigma_p = \frac{2}{3} \sigma_y.$$

Noting that $\epsilon|_{\sigma_p = \frac{2}{3}\sigma_y} = \frac{2}{3} \frac{\sigma_y}{E}$

$$C_1 = 0.513 \frac{\sigma_y}{E}$$

one finally obtains

$$\epsilon = \frac{\sigma_y}{4.5E} \left[2.306 + \ln \left| \frac{\sigma/\sigma_y}{1-\sigma/\sigma_y} \right| \right] \qquad (11)$$

Eq. (11) depicts the stress-strain curve above the proportional limit up to the yield strength, corresponding to Eq. (10). Stress-strain curves based on this equation are plotted as dashed curves in Figs. (2) to (5), for comparison with measured curves. Agreement is seen to be reasonable.

At incipient buckling, σ becomes $(\sigma_{cr})_t$ in Eq. (10), i.e.,

$$E_t = 4.5\ E\ \left[\ \frac{(\sigma_{cr})_t}{\sigma_y}\left\{1 - \frac{(\sigma_{cr})_t}{\sigma_y}\right\}\ \right] \qquad (12)$$

Substituting Eq. (12) into Eqs. (2) and (8),

$$(\sigma_x)_t = 4.5\ \frac{(\sigma_{cr})_t}{\sigma_y}\left[\ 1 - \frac{(\sigma_{cr})_t}{\sigma_y}\ \right]\sigma_x \qquad (13)$$

$$(\sigma_\phi)_t = 4.5\ \frac{(\sigma_{cr})_t}{\sigma_y}\left[\ 1 - \frac{(\sigma_{cr})_t}{\sigma_y}\ \right]\sigma_\phi \qquad (14)$$

Eq. (4) together with Eqs. (13) and (14) becomes

$$(\sigma_{cr})_t = 4.5\ \frac{(\sigma_{cr})_t}{\sigma_y}\left[\ 1 - \frac{(\sigma_{cr})_t}{\sigma_y}\ \right](\sigma_{cr})_E$$

and finally the torsional-flexural buckling stress in the inelastic domain becomes

$$(\sigma_{cr})_t = \sigma_y\left[1 - \frac{\sigma_y}{4.5\ (\sigma_{cr})_E}\right] \qquad (15)$$

where $(\sigma_{cr})_E$ is the elastic critical torsional-flexural buckling stress computed by Eq. (1a).

One obtains the same result by defining an effective slenderness ratio as follows.

In flexural buckling, if one knows the slenderness ratio, λ/r, one can compute the buckling stress

$$\sigma_{cr} = (\sigma_x)_E\ \frac{E_t}{E} = \frac{\pi^2\ E}{(\lambda/r)^2}\ \frac{E_t}{E}$$

in which $(\sigma_x)_E$ is the computed elastic Euler stress, which is higher than the actual buckling stress in the inelastic range.

If one equates $(\sigma_{cr})_t$ of torsional-flexural buckling to the above flexural buckling stress and solves the resulting equation for (λ/r), one gets the effective slenderness ratio; or conversely, one can compute the torsional-flexural buckling stress if one knows the effective slenderness ratio, $(\lambda/r)_{eff}$.

$$(\sigma_{cr})_t = \frac{\pi^2 E_t}{(\lambda/r)^2_{eff}} \tag{16}$$

Rewriting Eq. (16) analogously to the flexural case, one obtains

$$(\sigma_{cr})_t = \frac{E_t}{E} \frac{\pi^2 E}{(\lambda/r)^2_{eff}} \tag{17}$$

Then

$$\frac{\pi^2 E}{(\lambda/r)^2_{eff}} \approx (\sigma_{cr})_E \tag{18}$$

which is the computed elastic torsional-flexural buckling stress given by Eq. (1a). Therefore $(\lambda/r)_{eff}$ can be computed by

$$(\frac{\lambda}{r})^2_{eff} = \frac{\pi^2 E}{(\sigma_{cr})_E} \tag{19}$$

In the elastic domain, i.e., below the proportional limit, Eq. (19) gives the actual elastic torsional-flexural buckling stress.

Substituting Eq. (10) and (19) into Eq. (17),

$$(\sigma_{cr})_t = 4.5 \frac{(\sigma_{cr})_t}{\sigma_y} [\, 1 - \frac{(\sigma_{cr})_t}{\sigma_y}](\sigma_{cr})_E$$

and finally

$$(\sigma_{cr})_t = \sigma_y [\, 1 - \frac{\sigma_y}{4.5\ (\sigma_{cr})_E}\,] \tag{15}$$

as before.

Both approaches are based on the assumption expressed in Eq. (5). However, the physical meaning is better visualized in the first derivation.

It is now possible to extend the calculation procedures of the elastic case into the inelastic range and by applying Eq. (15) to obtain the critical torsional-flexural buckling stress in the inelastic range. The computed values in Table II are based on Eq. (15).

EXPERIMENTAL INVESTIGATION

The purpose of the experimental investigation was to verify the basic theory in the foregoing. Altogether, 30 tests were conducted on specimens having various sectional shapes and dimensions.

The main parameters which were considered in choosing specimens are as follows:

1. w/t ratio of the plate elements of specimens.

As this ratio increases, there may be local buckling prior to the over-all column buckling under axial compression. For the present investigation, the w/t ratios were chosen such that premature local buckling was avoided. Within such range of w/t ratios, a variety of cross-sectional dimensions were designed.

2. Wall-thickness.

If wall thickness is sufficiently small, the torsional rigidity of the cross-section is correspondingly reduced and the buckling load is so low that the average compressive stress cannot reach the inelastic domain. Therefore, steel

sheet thicknesses of 10 to 13 gages were selected.

3. Yield strength of material.

As discussed in the basic theory, the basic yield strength of the material is of great consequence to the column buckling stress and also to the local buckling. Hence, materials having relatively low yield strength were used.

4. Shape of specimen.

Tests were confined to shapes having singly symmetrical sections, to which most of the commonly used shapes belong.

5. End conditions.

Fully fixed end conditions were chosen. This was to eliminate the complex end fittings necessary for testing column with other end conditions. Moreover, the simpler the arrangement of the end restraints, the less error would be involved in aligning the specimen.

Specimens and Test Procedure

Specimens are grouped into four categories: plain equal legged angles, lipped angles, plain channels and hat sections. The cross-sectional configuration is shown in Fig. 1. A summary of specimen shapes and their dimensions is given in Table 1.

All tests were conducted on columns with length less than 70 in. The fixed end conditions were achieved by welding steel plates of 3/8 to 1/2 in. thickness to both ends of the specimen, which were then set in hydrostone placed on the base and head of the test machine.

The materials used for the specimens were 10 gage hot rolled sheets and 12 and 13 gage cold reduced sheets. Column specimens were made by press braking at a local shop (Champion Sheet Metal Co., Cortland, N.Y.) to specified dimensions.

Stub column compression tests were made to evaluate the effective over-all stress-strain relationship of the specimens. A stub column is a short piece cut from the specimen to be tested. While details of the stub column test procedure are fully described elsewhere,[5] a brief explanation will be given below.

A schematical setup of a stub column test is depicted in Fig. 7. The specimen was surrounded by hydrostone cast in a steel pipe to limit plate local buckling. SR-4 strain gages were attached to the plate elements of the stub column and were then coated with wax in order to secure waterproof. Each strain gage was then covered with a half section of metal tube approximately 7 1/2 in. long split longitudinally. Water-proofing wax was again coated along the tubing. The specimens were then greased and wrapped in aluminum foil to minimize friction between the surface of the specimen and hydrostone. The entire assemblage was cast in hydrostone contained in a 4 in. steel pipe or 6 in. square tube of 7 1/2 in. length, depending on the size of the specimen. Before the stub column was placed in hydrostone, the ends were cut so that the end surfaces were perpendicular to the longitudinal axis; both ends were milled to smooth surfaces

after the specimen was cast in hydrostone. After the hydrostone had hardened completely and heat generated was dissipated, the specimen was brought to test.

In testing, the specimen was placed on a milled plate of 1-1 1/2 in. thickness which was fixed by hydrostone on the base of the testing machine. The plate was checked to be horizontal by means of a bubble tube. Under the head of the machine, the same arrangement was made.

The stub column cross-sectional area was determined accurately by measuring the weight and length of the specimen. The average stresses were computed and plotted against the average strain readings of the strain gages. Typical stress-strain curves are shown in Figs. 2, 3, 4 and 5. (Others are included in Appendix A.)

Basic instrumentation of the column tests consisted of two needles attached to the column walls at mid-height and a circular ring with scale increments of 0.01 inch to measure the rotation of the column as indicated by the movement of the needles; dial gages to measure the column deflection at mid-height; and electrical resistance strain gages at certain points on the column walls mainly to check the column alignment. The vertical alignment was first checked by a plumb-bob and also by a bubble tube.

The column specimens were loaded in a hydraulic test machine with load increment of 500 to 2000 lbs., depending on the specimen and the predicted buckling load. As the buckling load was approached, the load increment was reduced. Typical test setup and testing are shown in Figs. 8 and 9.

The applied average stresses, P/A, were plotted against the measured rotations at mid-height and against the deflections in the direction perpendicular to the axis of symmetry.

Discussion of Results

Typical stress-deformation curves are shown in Figs. 10, 11, 12 and 13. (The curves for all other specimens are given in Appendix B.) It is seen that the behavior of the specimens is similar to that of an axially loaded column with imperfections. The stress-deformation curves show gradually increasing rotations and simultaneous lateral deflections in the intermediate range, with rapidly increasing deformations as the buckling stress was approached.

The stress-deformation curves show that failure occurred at the stresses in the inelastic domain. They also show that there was no apparent post-buckling strength. This confirms again that post-buckling strength depends on $\frac{\sigma_y}{\sigma_{cr}}$ ratio, i.e., the greater the ratio, the smaller will be the difference between the buckling load and the failure load, as reported before. Since the inelastic buckling stress is close to the yielding strength, post-buckling strength cannot be expected.

An interesting discussion was presented by N. J. Hoff[4] concerning the definition of buckling load of an inelastic column. He observed that there is no definition of experimental buckling load in a manner acceptable to all research men. The maximum load has the most clear-cut physical significance and is also easily observed experimentally. So-called critical load is based on the classical concept of

stability and is obtained as the Eigenvalue of the load at which neighboring, slightly deflected equilibrium configuration exists simultaneously with the initial configuration. The extension of this concept leads to the double modulus load which gives a value higher than the maximum inelastic column load. The tangent modulus load has the merit that it can be easily calculated as soon as the stress-strain curve is known. It also agrees, on the average, with the maximum load observed with actual, somewhat imperfect columns.

In view of this, the maximum observed stresses (i.e., the P/A at maximum load) are given in Table II for comparison with the computed values. A quick over-all comparison is presented in Fig. 14. A non-dimensional curve is plotted taking $\Delta = \frac{1}{\pi}\sqrt{\frac{\sigma_y}{E}}\,(\lambda/r)_{eff}$ vs. $\frac{\sigma_{cr}}{\sigma_y}$ as shown. The scattering of the experimental data is not large in general, and the agreement with the theoretical curve is close.

It is seen that the only significant unconservative deviations from the C = 4.5 curve (up to 15%) occurred for three hat sections. Hat sections had the largest number of corners of all sections tested and therefore, probably the largest imperfections. This is confirmed by the over-all shape of the load-deformation curves of the hat section columns.

For comparison, $(\sigma_{cr})_t$ based on C = 4.5 are computed and are listed in Table II. Two additional curves based on C = 5 and C = 4 are also plotted in Fig. 14, the latter corresponding to CRC column curve except (L/r) is $(\lambda/r)_{eff}$

in this case. The buckling stresses of angle sections are closer to the values computed by using C = 5, while those of lipped angle and hat sections are closer to the values by C = 4. This is to be expected since the stress-strain curve for angle section is more of the sharp yielding type, while for lipped angle and hat sections it is more of a gradually yielding pattern.

It is seen from Fig. 14 that, if desired for simplicity, one may get more conservative, yet reasonable, torsional-flexural buckling stresses for all tested shapes by replacing 4.5 by 4.0 in Eq. (15).

SUMMARY AND CONCLUSIONS

1. The most difficult factor in the analysis of inelastic torsional-flexural buckling is the determination of the appropriate tangent modulus of shear. In order to simplify the computations and yet obtain reasonably accurate value of computed buckling stress, an assumption was made in Eq. (7). This makes possible the simple extension of the computation procedure of the elastic case into the inelastic range.

2. As the best fit to stub column test results, the tangent modulus, E_t, was expressed in the parabolic form:

$$E_t = 4.5\, E\, \frac{\sigma}{\sigma_y}\left(1 - \frac{\sigma}{\sigma_y}\right)$$

to represent the over-all stress-strain relationship of the columns.

3. The torsional-flexural buckling stress in the inelastic range (i.e., for $(\sigma_{cr})_t \geq \sigma_p = \frac{2}{3}\sigma_y$) can be computed by the following formula:

$$(\sigma_{cr})_t = \sigma_y \left[1 - \frac{\sigma_y}{4.5(\sigma_{cr})_E}\right] \qquad (15)$$

in which

$$(\sigma_{cr})_E = \frac{1}{2\left[1-\left(\frac{x_o}{r_o}\right)^2\right]} \left[\sigma_x + \sigma_\phi - \sqrt{(\sigma_x + \sigma_\phi)^2 - 4\left[1-\left(\frac{x_o}{r_o}\right)^2\right]\sigma_x \cdot \sigma_\phi}\right]$$

4. Thirty tests on full size columns were made. The experimental results agreed with the computed values within a close range.

5. More conservative values of buckling stress may be obtained by replacing the numerical factor 4.5 in Eq. (15) by 4. In this case, if $(\lambda/r)_{eff}$ is used in place of (L/r), the CRC parabolic column curve for flexural buckling can also be employed for thin-walled members which buckle in a torsional-flexural mode.

REFERENCES

1. Timoshenko, S. P., and J. M. Gere. Theory of Elastic Stability, McGraw-Hill, 1961.

2. Bleich, F. Buckling Strength of Metal Structures, McGraw-Hill, 1952.

3. Chajes, A. and Winter, G., First Progress Report on Torsional-Flexural Buckling of Thin-Walled Open Sections, 1963.

4. Hoff, N. J. Buckling and Stability, Journal of Royal Aeronautical Society, v. 58, p. 1, January, 1954.

5. Karren, K. Effects of Cold-Forming on Light-gage Steel Members, Sixth Progress Report, Dept. of Structural Eng., Cornell University.

6. Galambos, T. V. and Y. Fukumoto. Inelastic Lateral-torsional Buckling of Beam-Columns, Fritz Engineering Lab. Report No. 205A.34.

7. Galambos, T. V., and P. F. Adams and Y. Fukumoto. Further Studies on the Lateral-Torsional Buckling of Steel Beam-Columns, Fritz Eng. Lab Report No. 205A.36.

8. Bernstiel, C., and Michalos, J. Ultimate Load of H-Columns under Biaxial Bending, J. Struc. Division, Trans. ASCE, April, 1963.

9. Roik, K. Biegedrillknicken mittig gedrückter Stäbe mit offenem Profil im unelastischen Bereich, Der Stahlbau, 1956, p. 10.

10. Bijlaard, P. P., Fisher, G. P. Interaction of Column and Local Buckling, NACA TN 2640, 1952.

TABLE 1. SUMMARY OF SPECIMENS

Section	Specimen	Dimensions (in) a	b	c	t	L	σ_y (ksi)
Plain Angle	A-1	1.93			0.135	56.0	44.7
	A-2	1.83			0.135	40.0	44.7
	A-3	2.35			0.135	55.0	41.4
	A-4	2.39			0.135	55.0	41.4
	A-5	2.60			0.135	30.0	41.4
	A-6	1.438			0.103	39.98	30.0
Lipped Angle	LA-1	2.135	0.568		0.1365	40.0	47.0
	LA-2	2.635	0.8175		0.135	50.0	45.6
	LA-3	2.135	0.568		0.1365	65.02	41.0
	LA-4	2.635	0.8175		0.135	65.04	45.6
	LA-5	1.847	.8086		0.1028	59.97	31.7
	LA-6	2.007	.9166		0.103	49.98	31.7
	LA-7	1.584	0.780		0.0908	49.97	32.2
	LA-8	1.582	0.8125		0.103	50.4	34.25
	LA-9	1.675	0.825		0.090	49.97	32.2
Channel	CH-1	2.135	1.568		0.135	55.03	45.25
	CH-2	1.603	1.552		0.103	34.0	31.0
	CH-3	1.603	1.552		0.103	40.03	31.0
	CH-4	1.5468	1.5684		0.1032	60.05	31.0
	CH-5	2.057	2.069		0.103	60.0	30.4
	CH-6	2.068	1.829		0.1023	54.97	30.4
	CH-7	1.546	1.568		0.1045	50.03	31.0
	CH-8	2.047	1.819		0.1028	55.0	30.4
	CH-9	1.584	1.534		0.0866	45.0	31.0
Hat	HA-1	2.135	2.135	1.068	0.135	45.0	46.9
	HA-2	2.635	2.135	1.318	0.135	49.94	46.9
	HA-3	2.135	2.135	1.068	0.135	60.0	46.9
	HA-4	1.587	1.857	0.8085	0.103	50.03	36.5
	HA-5	1.581	1.811	0.775	0.090	50.0	36.5
	HA-6	2.098	2.058	1.059	0.1019	60.0	30.7

Note: Cross-sectional dimensions a, b and c denote inside middle-line dimensions.

TABLE 2 TEST RESULTS

Specimen		Buckling Stress (ksi)				
		Tested	Computed			
			C=4	% Diff.	C=4.5	% Diff.
Angle	A-1	38.31	35.6	- 7.07	36.65	- 4.53
	A-2	38.26	36.6	- 4.34	37.50	- 2.02
	A-3	33.20	28.5	-14.1	29.89	-11.10
	A-4	33.18	29.1	-12.3	30.43	- 9.04
	A-5	32.2	27.4	-14.9	28.90	-11.4
	A-6	22.49	23.8	+ 5.82	24.57	+ 8.25
Lipped Angle	LA-1	36.6	36.0	- 1.64	37.22	+ 2.31
	LA-2	34.6	37.9	+ 9.53	38.76	+10.8
	LA-3	30.3	30.9	+ 0.99	32.71	+ 8.0
	LA-4	30.23	29.6	- 2.08	31.28	+ 3.45
	LA-5	26.46	24.3	- 8.16	25.10	- 5.3
	LA-6	23.90	23.8	- 0.42	24.73	+ 7.0
	LA-7	24.96	25.7	+ 2.96	26.40	+ 5.45
	LA-8	27.17	28.0	+ 3.05	28.70	+ 5.23
	LA-9	27.05	25.5	- 5.74	26.21	- 0.34
Channel	CH-1	38.79	39.8	+ 0.05	40.82	+ 4.95
	CH-2	29.46	28.2	- 4.28	28.49	- 3.4
	CH-3	27.95	27.5	- 1.61	27.93	- 0.71
	CH-4	24.98	25.4	+ 1.68	25.98	- 3.85
	CH-5	25.24	25.8	+ 2.22	26.27	- 4.18
	CH-6	27.28	26.4	- 3.22	26.90	- 1.41
	CH-7	27.05	26.4	- 2.40	26.94	- 0.41
	CH-8	26.40	26.5	- 0.38	26.96	+ 2.1
	CH-9	26.73	26.6	- 0.487	27.13	+ 1.48
Hat	HA-1	38.19	38.7	+ 1.33	39.58	+ 3.52
	HA-2	38.94	38.9	- 0.10	39.72	+ 1.96
	HA-3	31.60	34.1	+ 7.91	34.95	+ 8.27
	HA-4	23.75	26.9	+13.7	28.00	+15.20
	HA-5	22.57	25.6	+13.4	26.83	+15.60
	HA-6	23.32	23.9	+ 2.42	24.68	+ 5.50

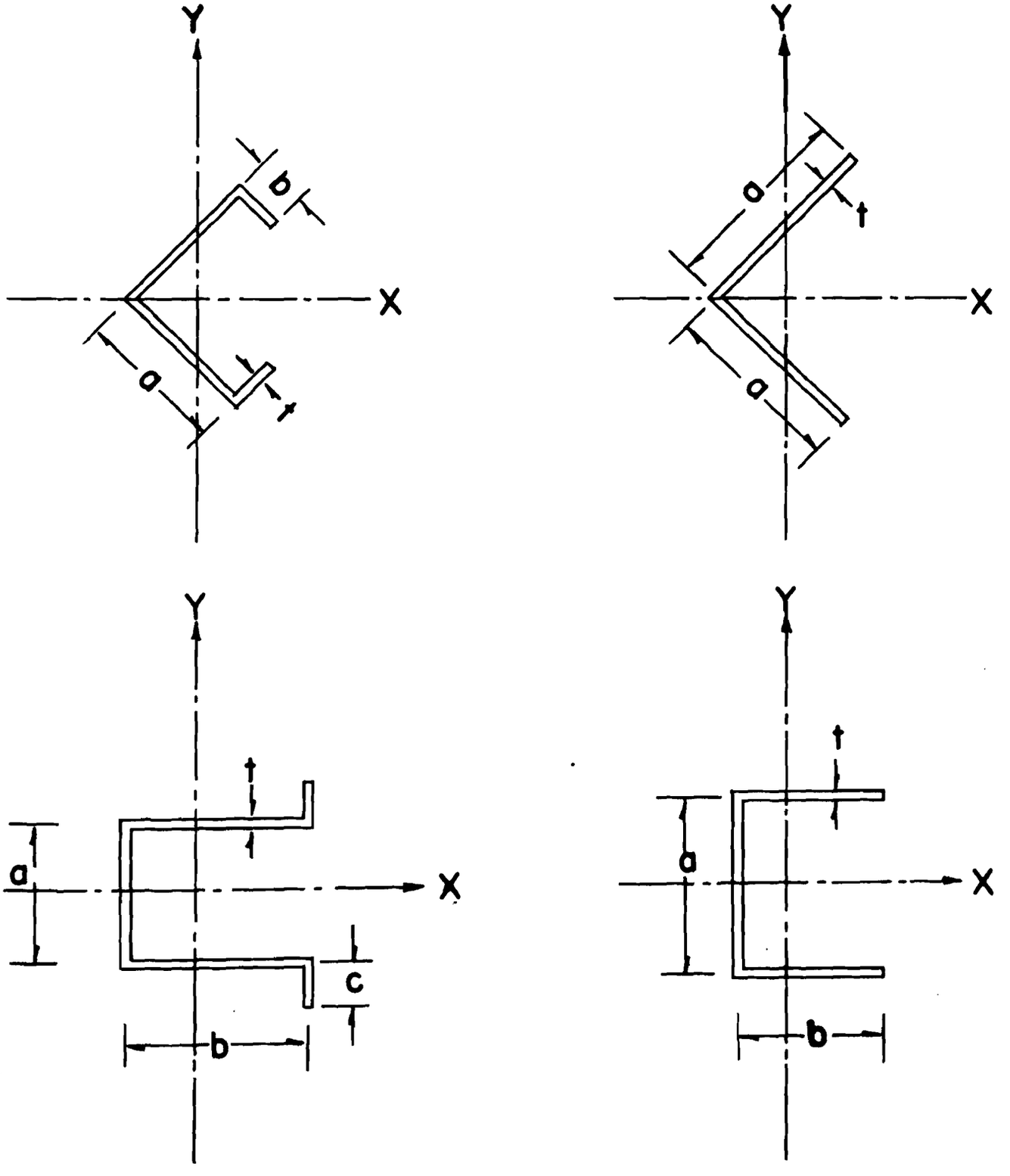

FIG.1. SINGLY SYMMETRICAL SECTIONS

Fig. 1

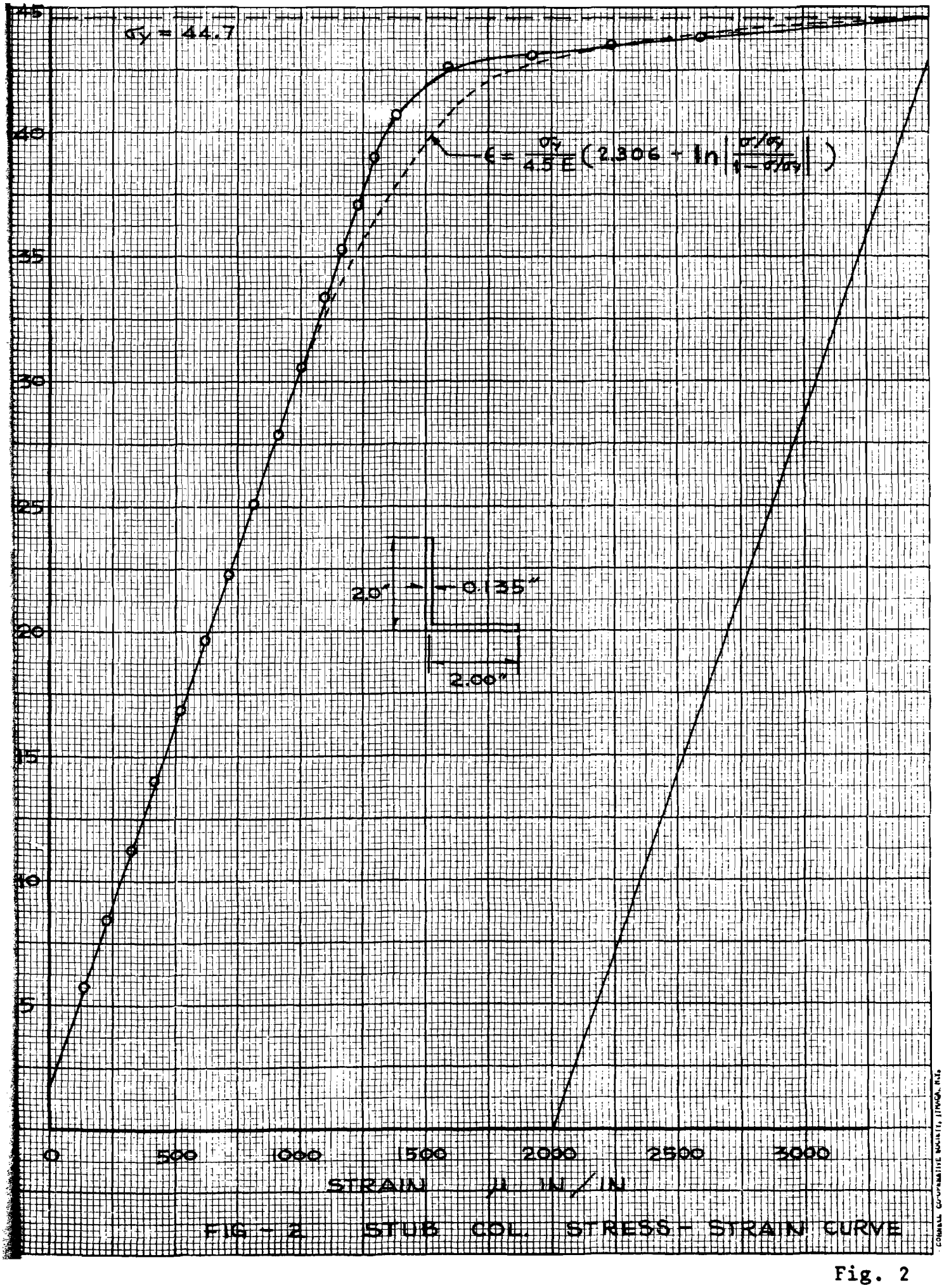

FIG - 2. STUB COL. STRESS - STRAIN CURVE

Fig. 2

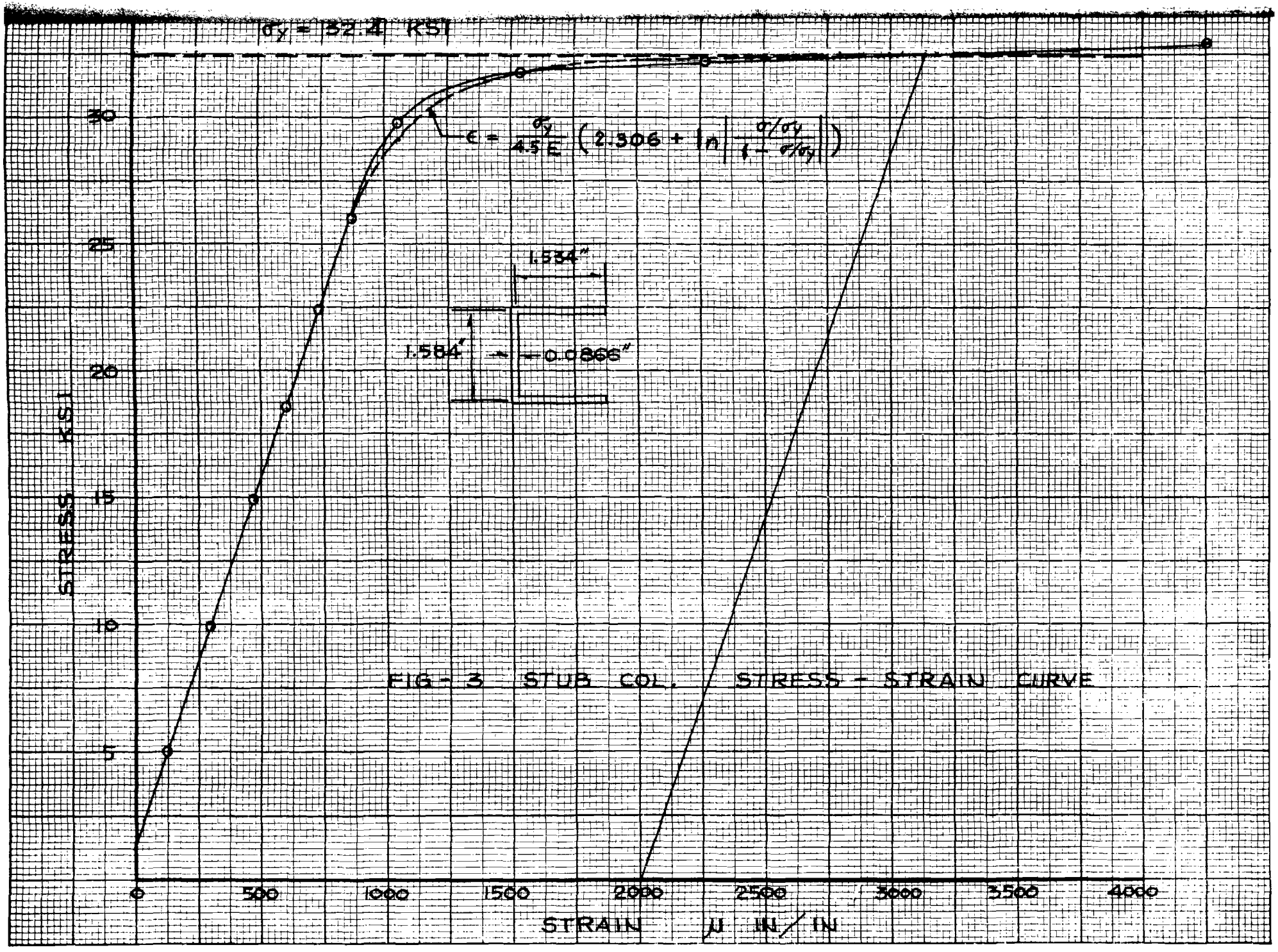

FIG - 3 STUB COL. STRESS - STRAIN CURVE

Fig. 3

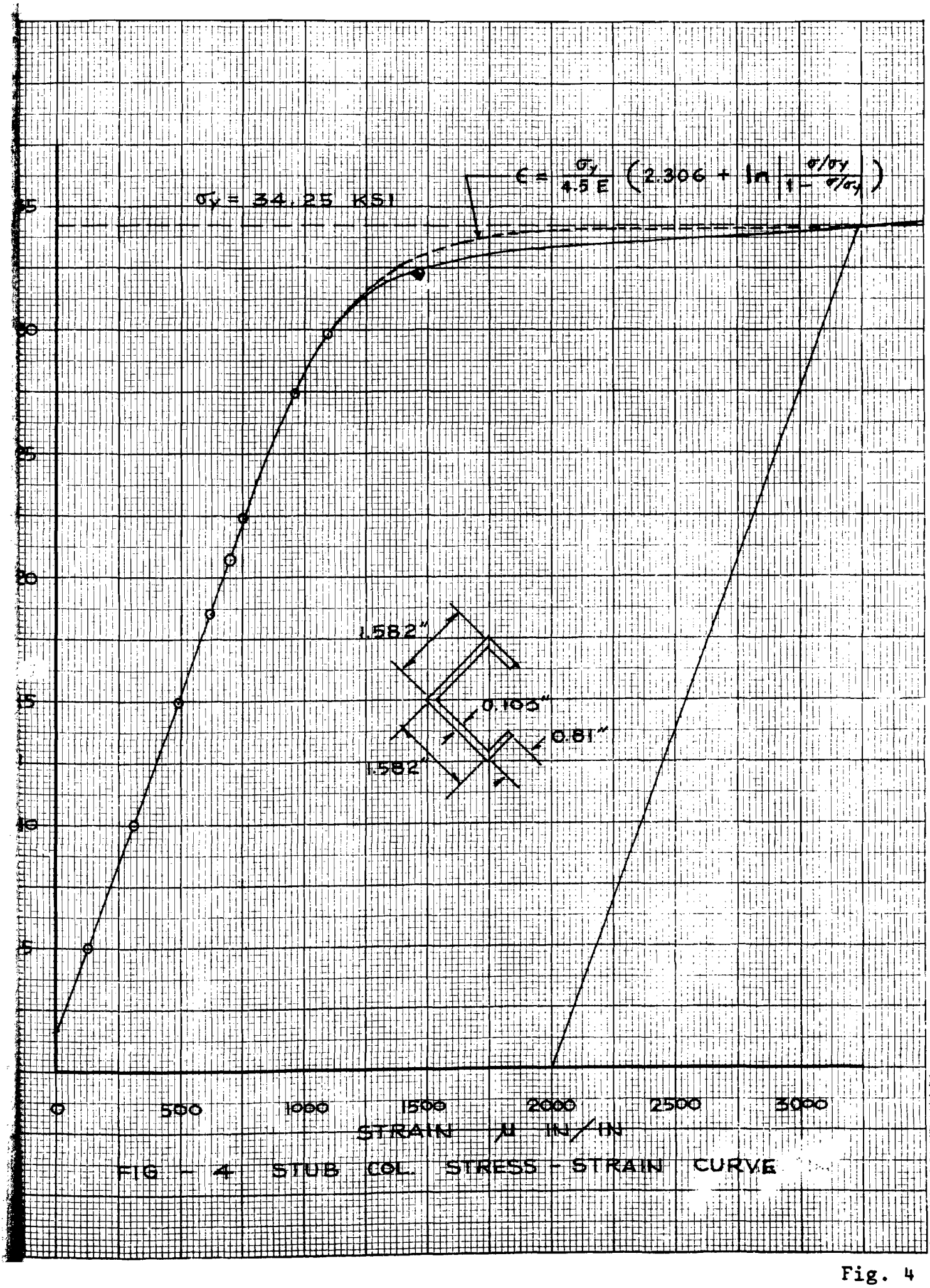

FIG - 4 STUB COL. STRESS - STRAIN CURVE

Fig. 4

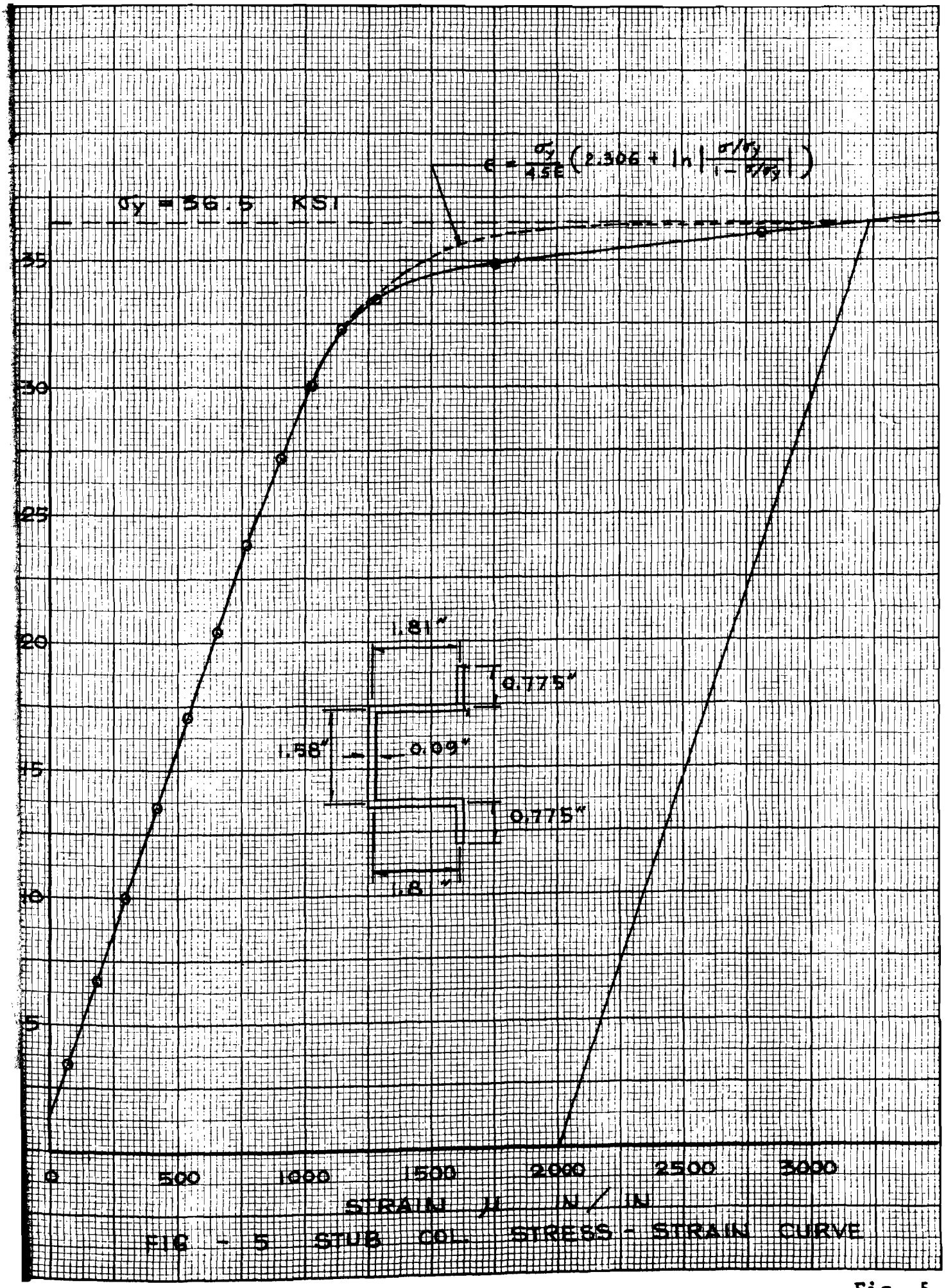

FIG - 5 STUB COL. STRESS - STRAIN CURVE

Fig. 5

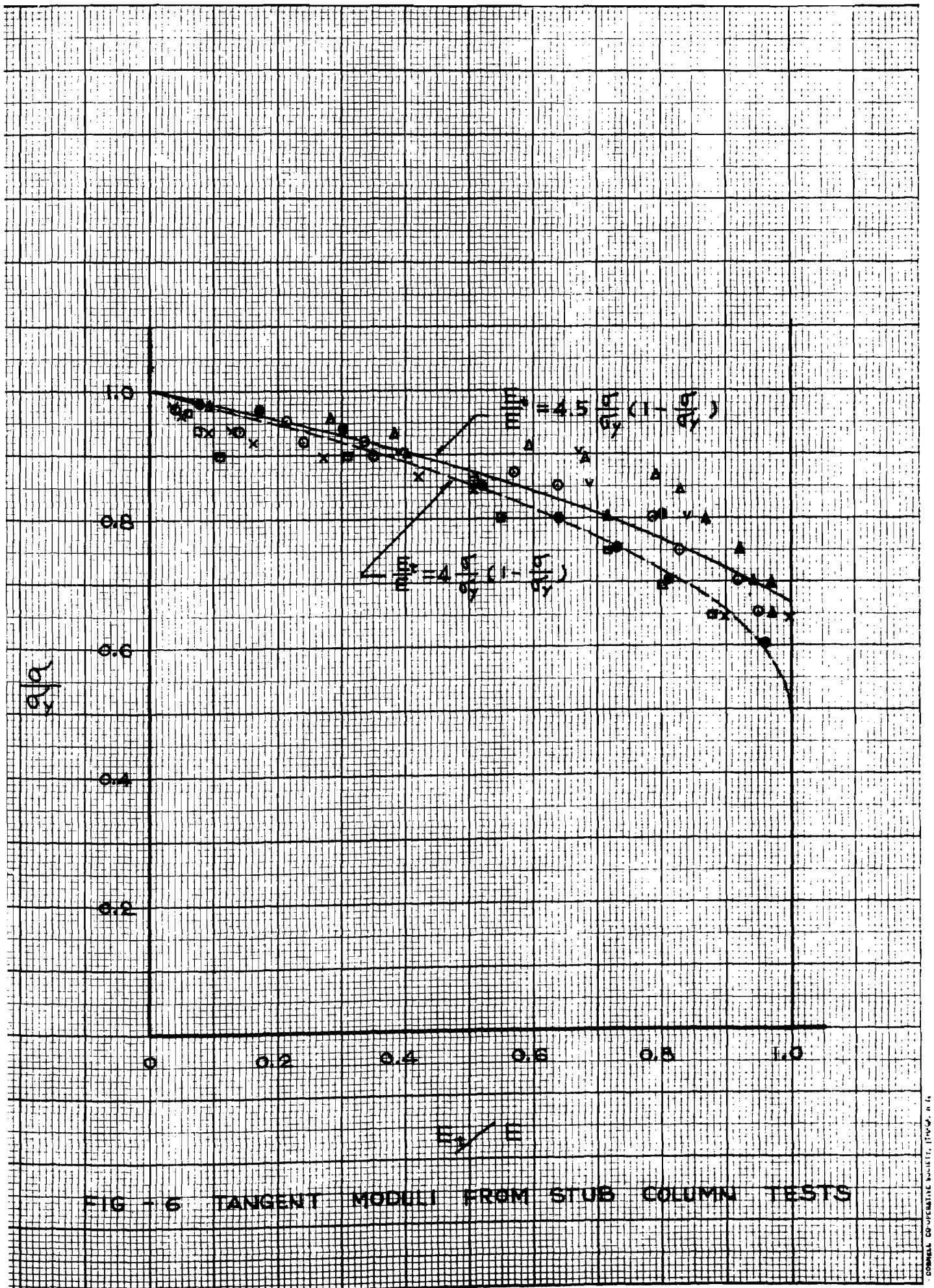

FIG - 6 TANGENT MODULI FROM STUB COLUMN TESTS

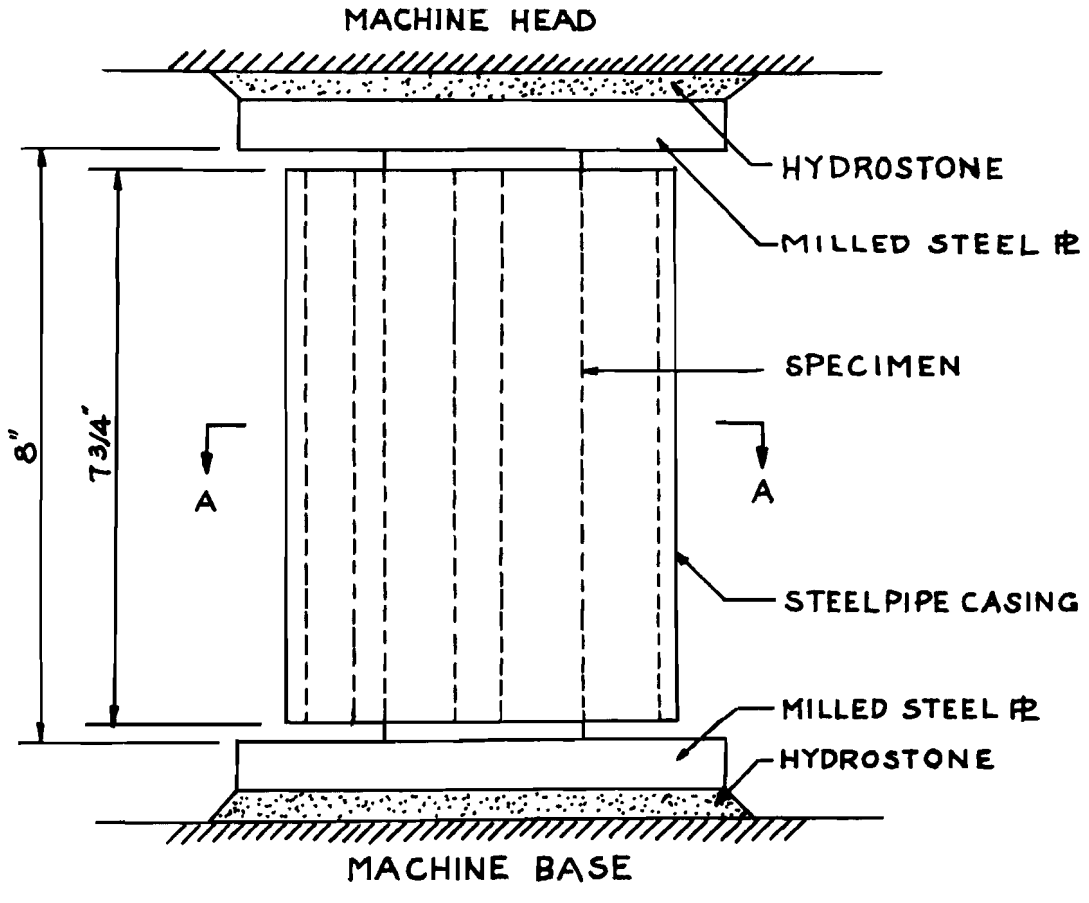

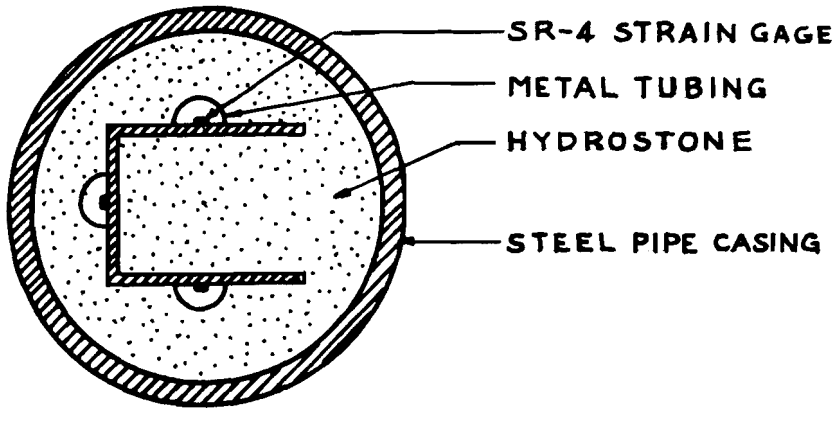

A - A

FIG. 7 STUB COLUMN TEST SET-UP

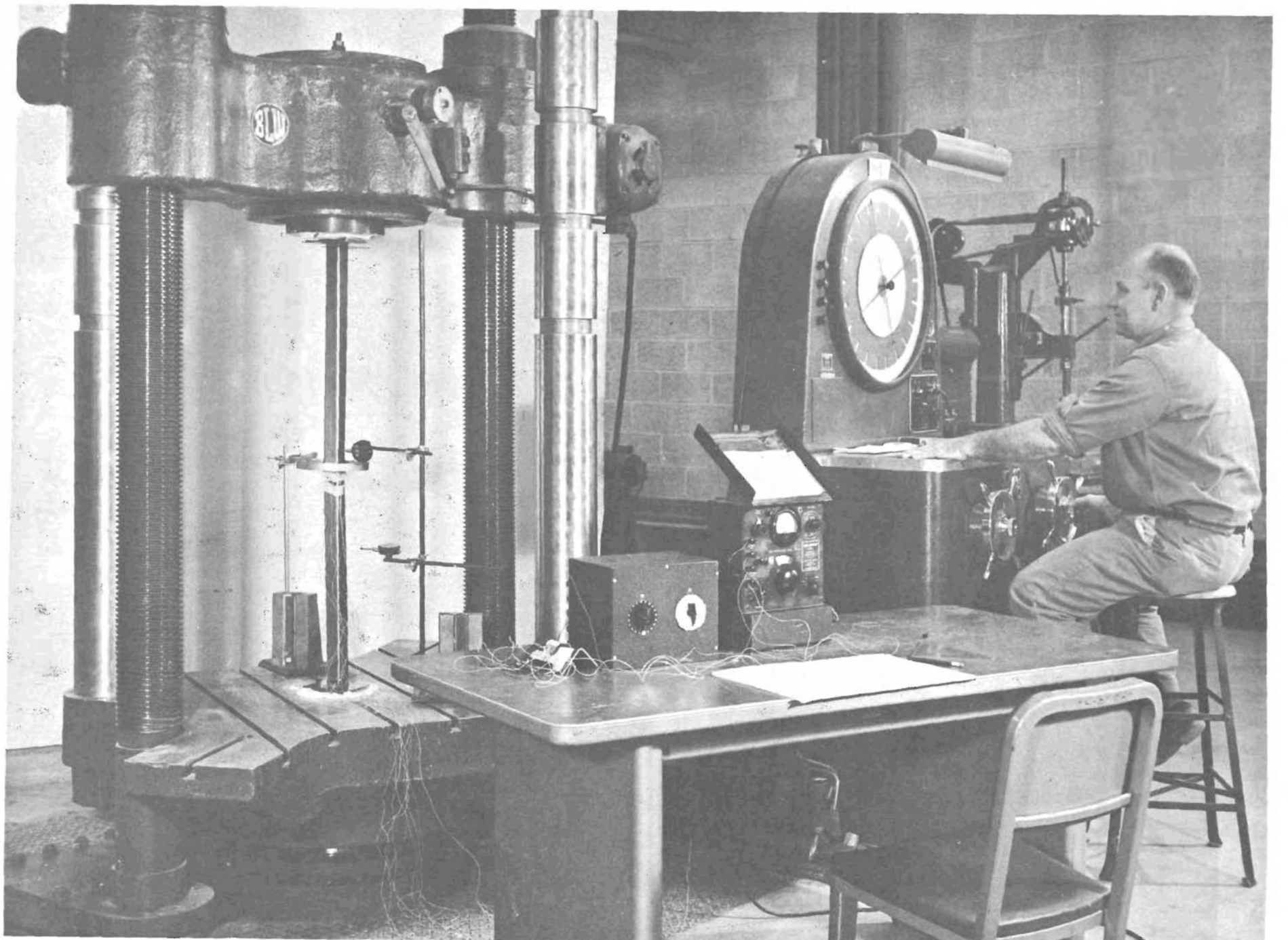

FIG. 8 COLUMN TEST SET-UP

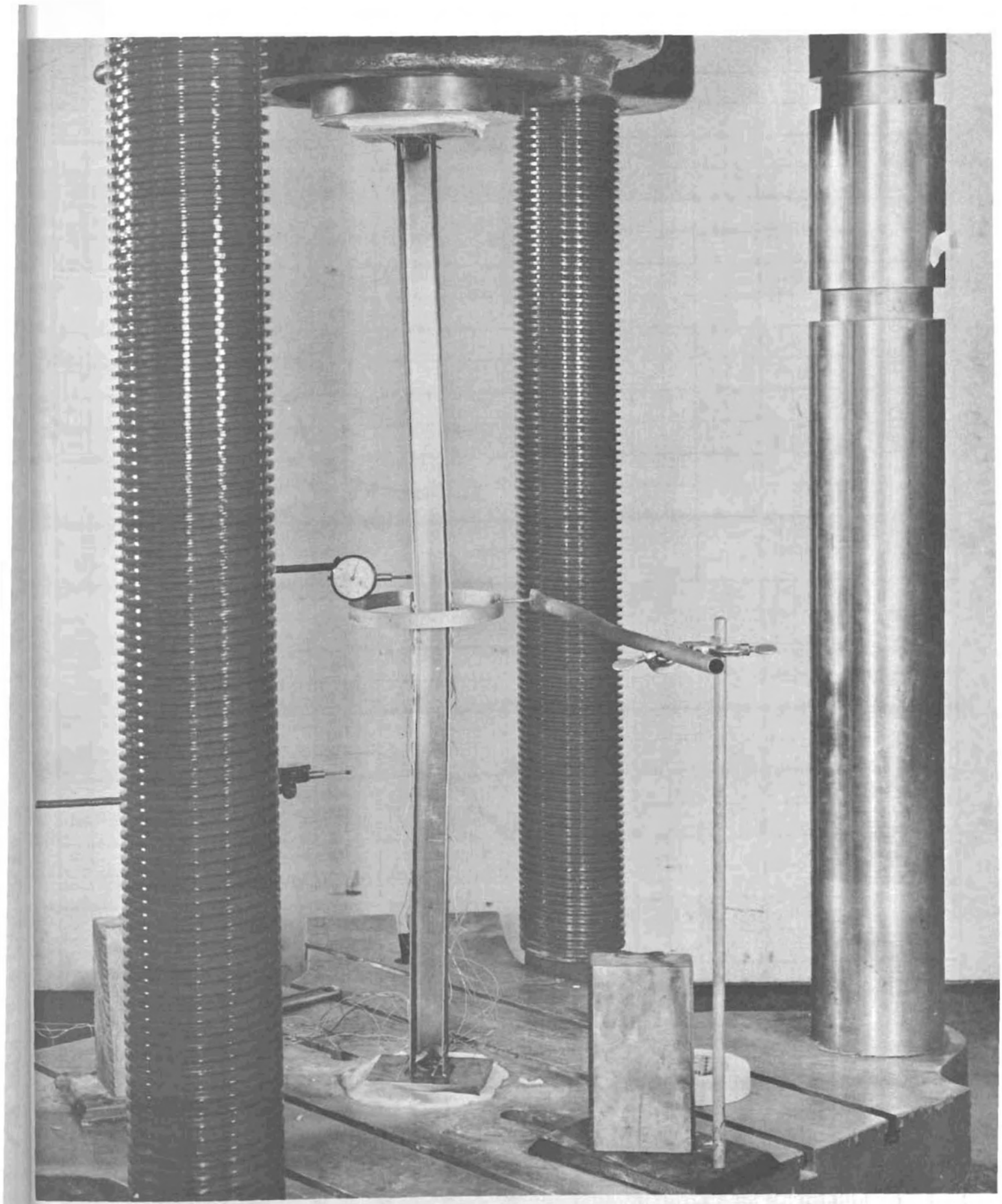

FIG. 9. COLUMN TEST (CHANNEL SECTION)

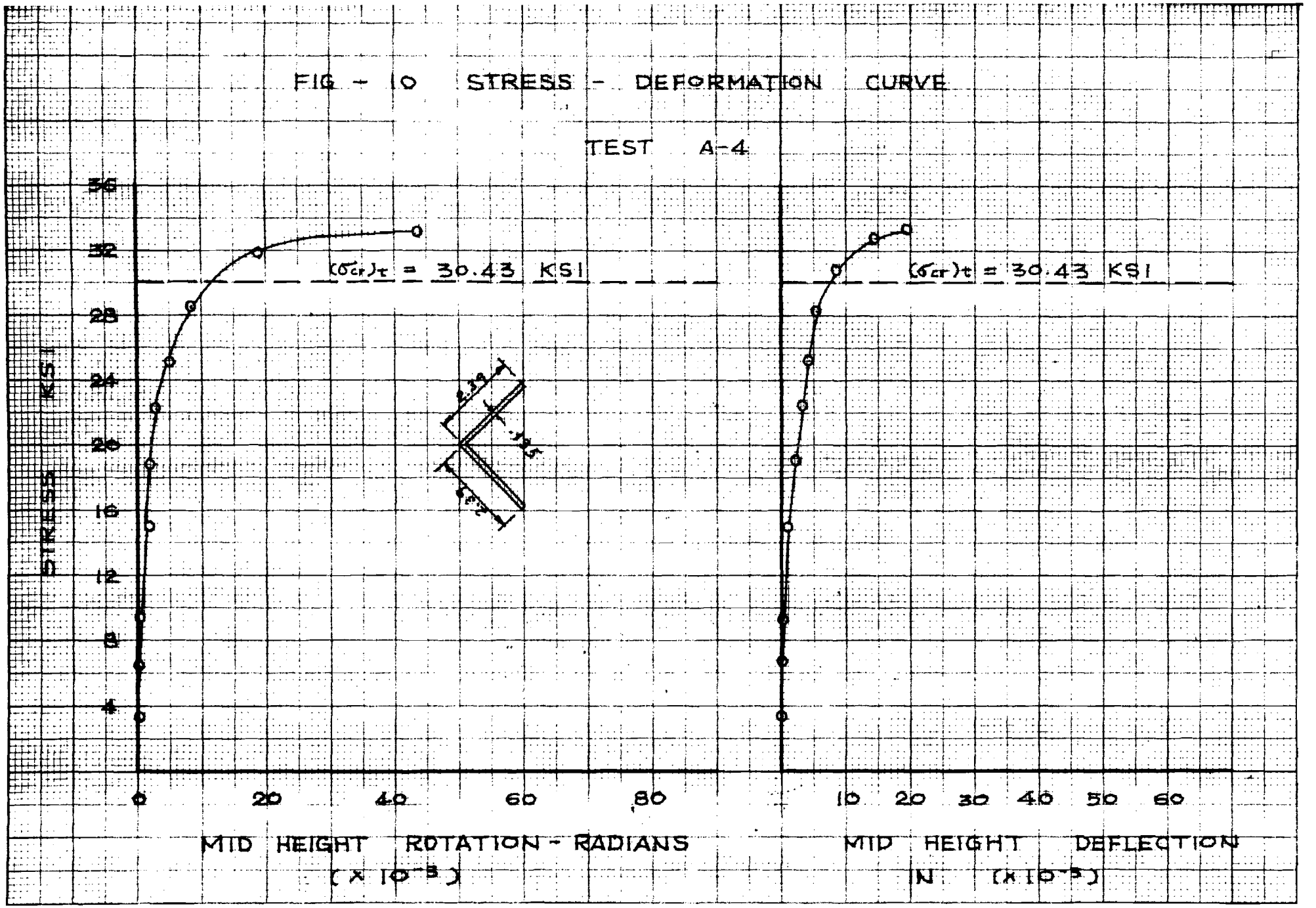
FIG - 10 STRESS - DEFORMATION CURVE
TEST A-4
STRESS KSI
36
32
28
24
20
16
12
8
4
$(\sigma_{cr})_t$ = 30.43 KSI
$(\sigma_{cr})_t$ = 30.43 KSI
0
20
40
60
80
10
20
30
40
50
60
MID HEIGHT ROTATION - RADIANS
(x 10^{-5})
MID HEIGHT DEFLECTION
IN (x 10^{-5})

Fig. 10

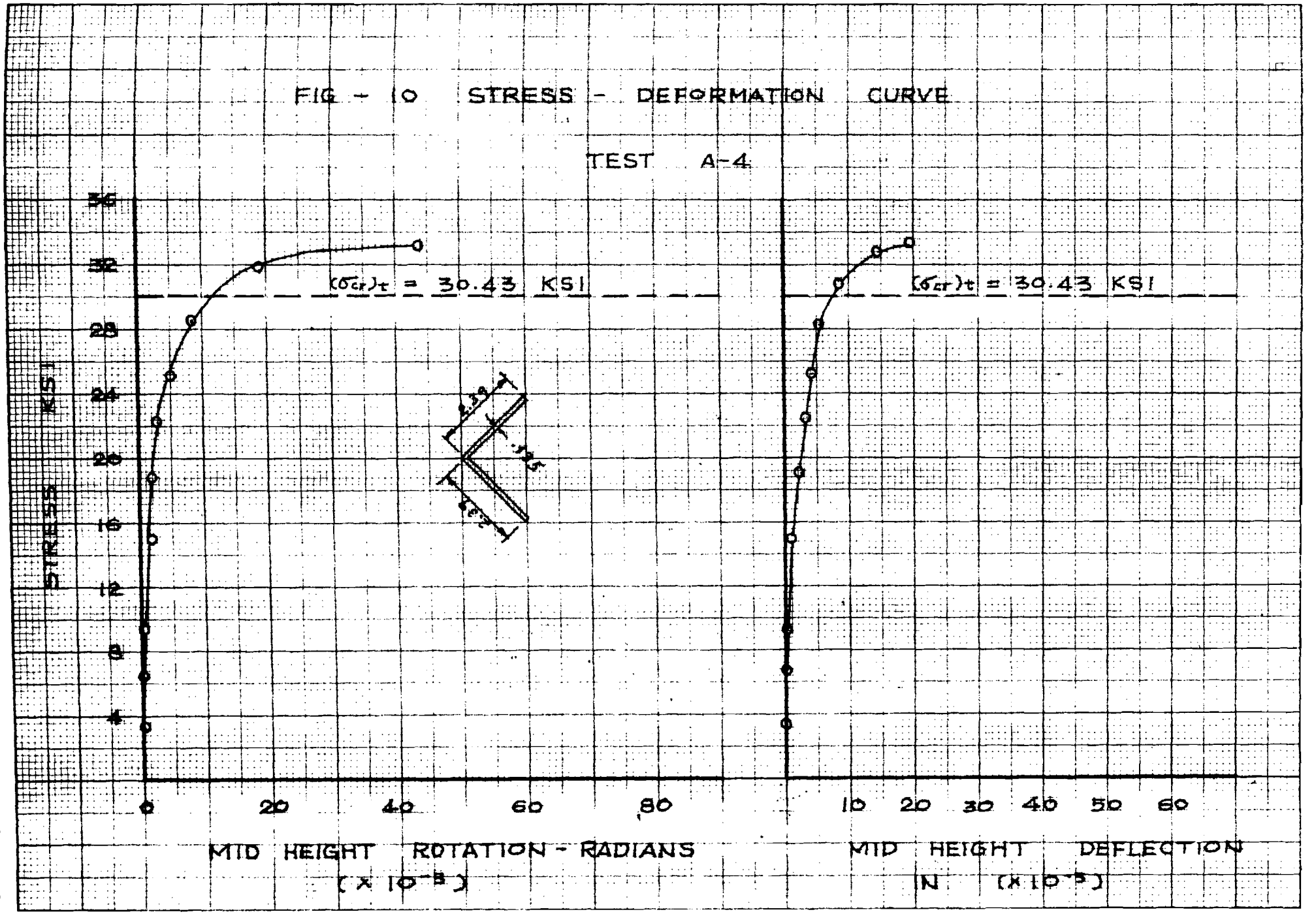
FIG - 10 STRESS - DEFORMATION CURVE
TEST A-4
STRESS - KSI
56
32
28
24
20
16
12
8
4
$(\sigma_{cr})_t$ = 30.43 KSI
$(\sigma_{cr})_t$ = 30.43 KSI
0
20
40
60
80
10
20
30
40
50
60
MID HEIGHT ROTATION - RADIANS
(x 10^{-5})
MID HEIGHT DEFLECTION
IN (x 10^{-5})

Fig. 10

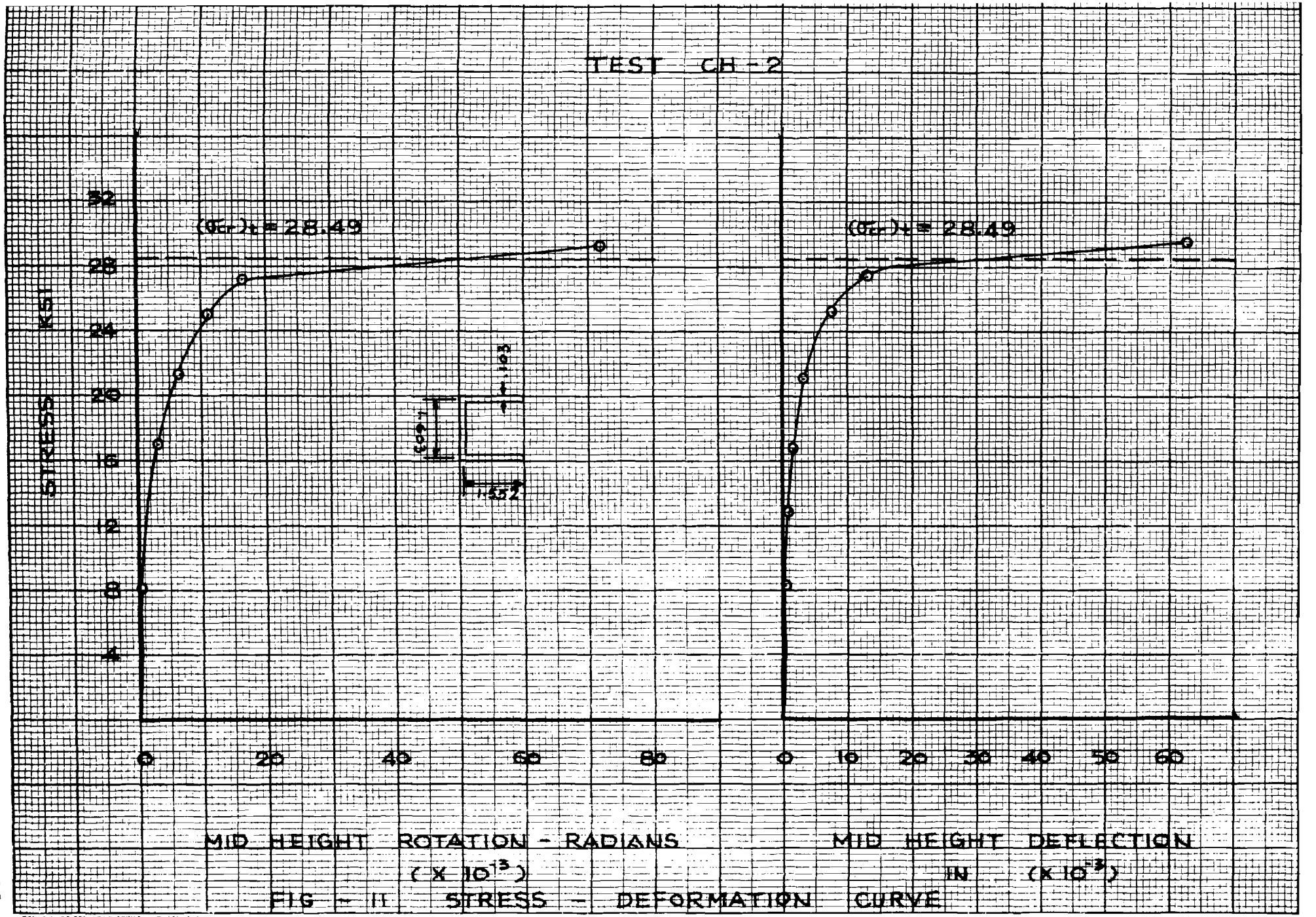

FIG - 11 STRESS - DEFORMATION CURVE

Fig. 11

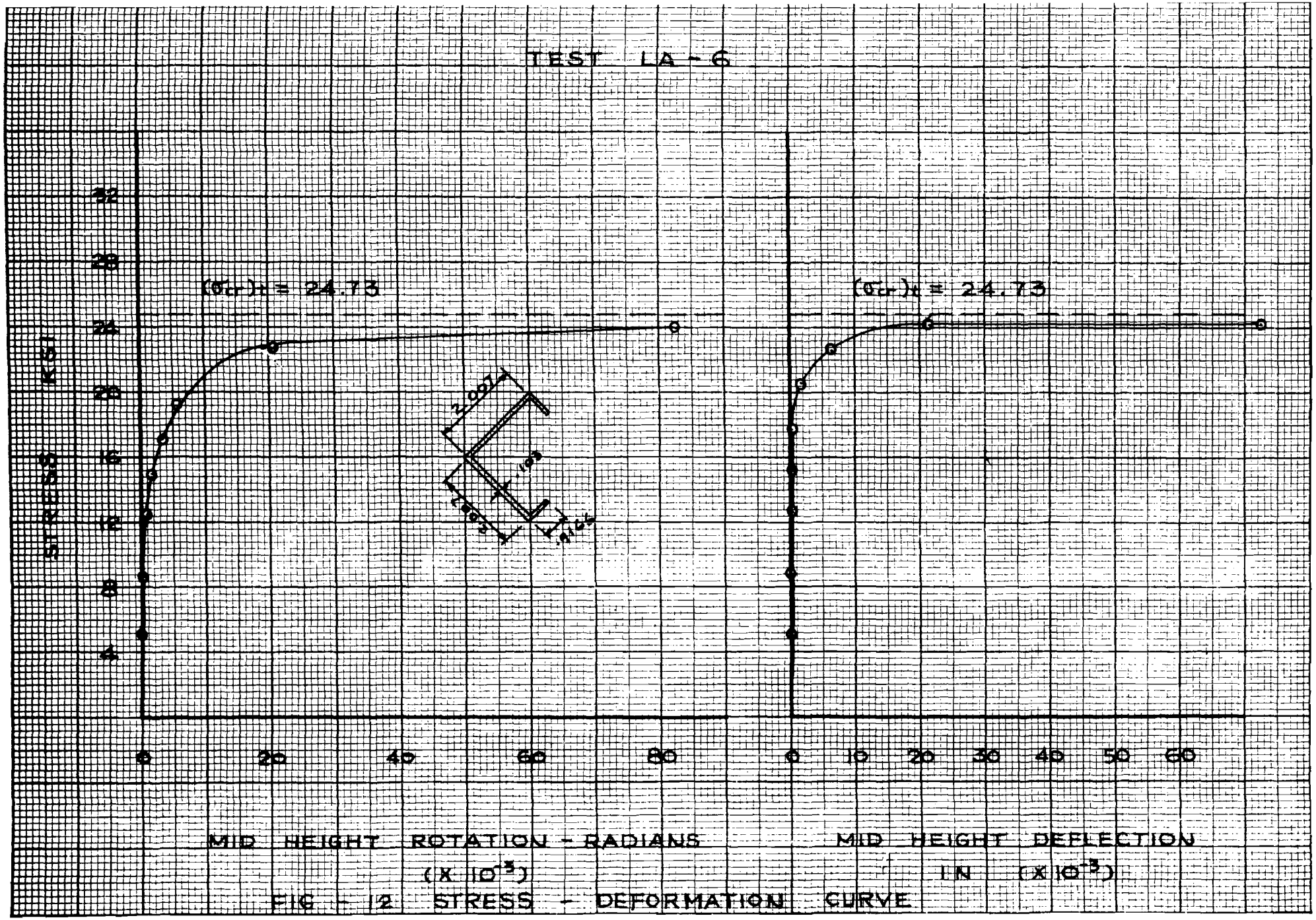

FIG - 12 STRESS - DEFORMATION CURVE

Fig. 12

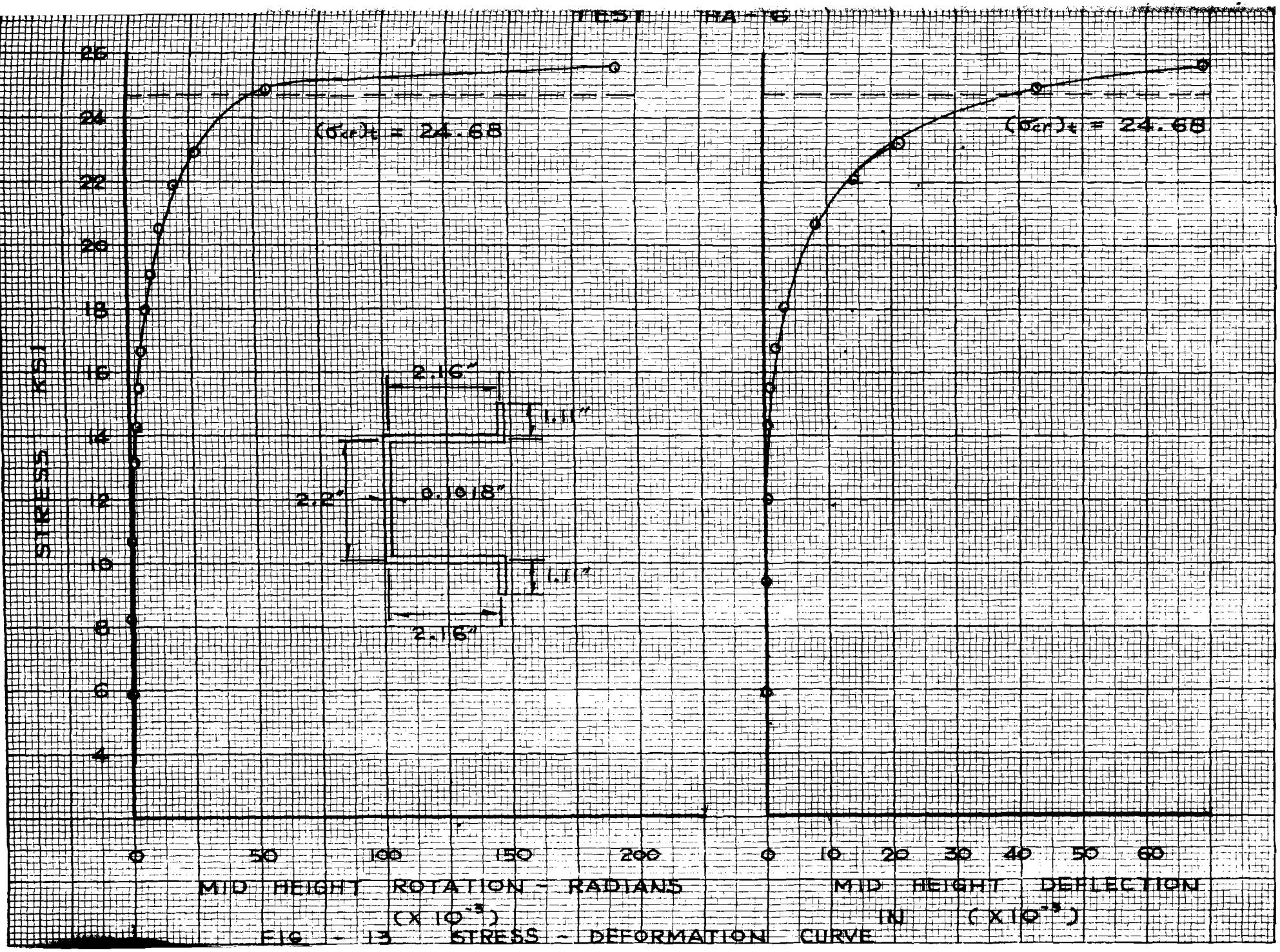

FIG. - 13 STRESS - DEFORMATION CURVE

Fig. 13

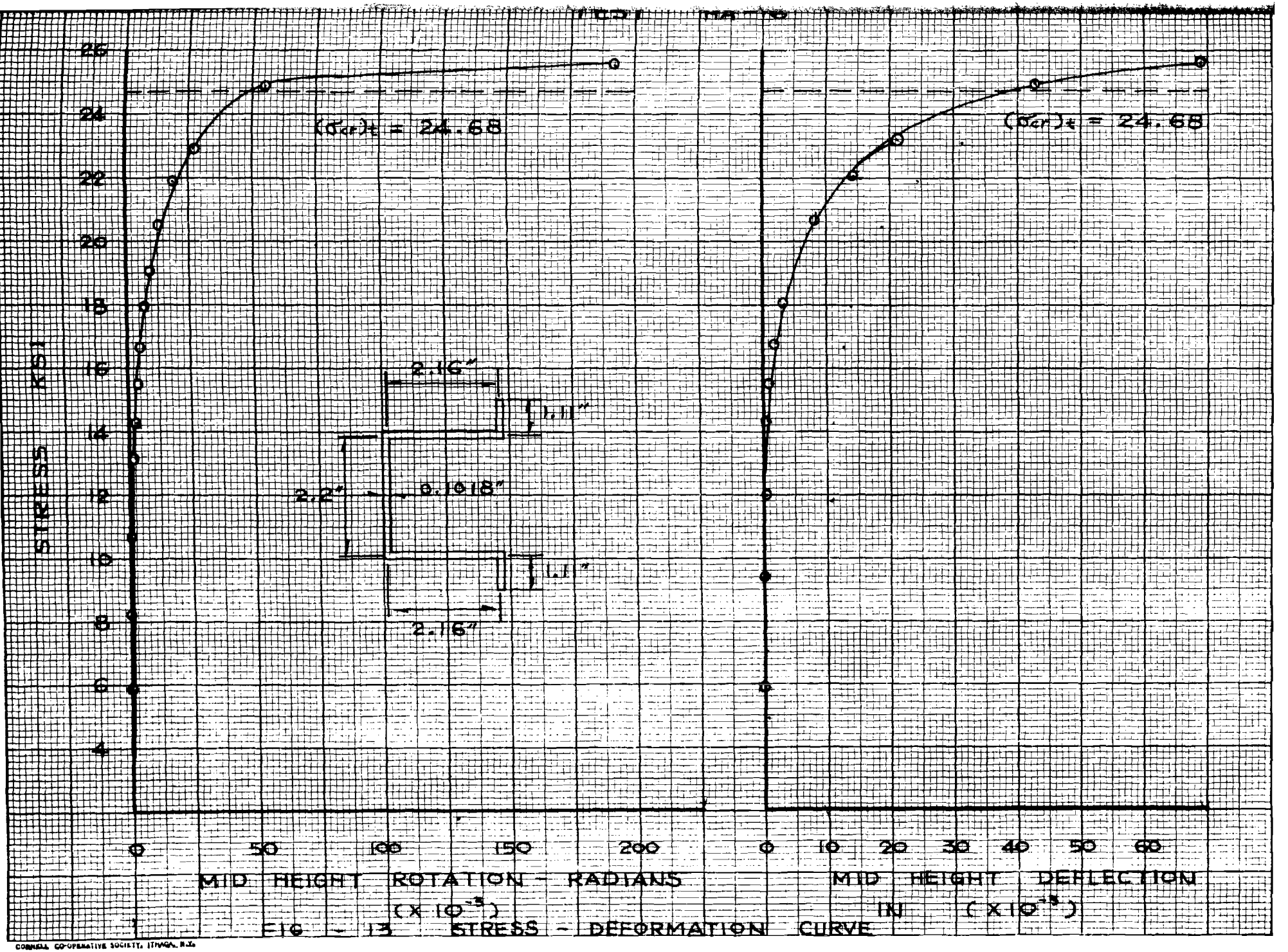

FIG. 13 STRESS - DEFORMATION CURVE

Fig. 13

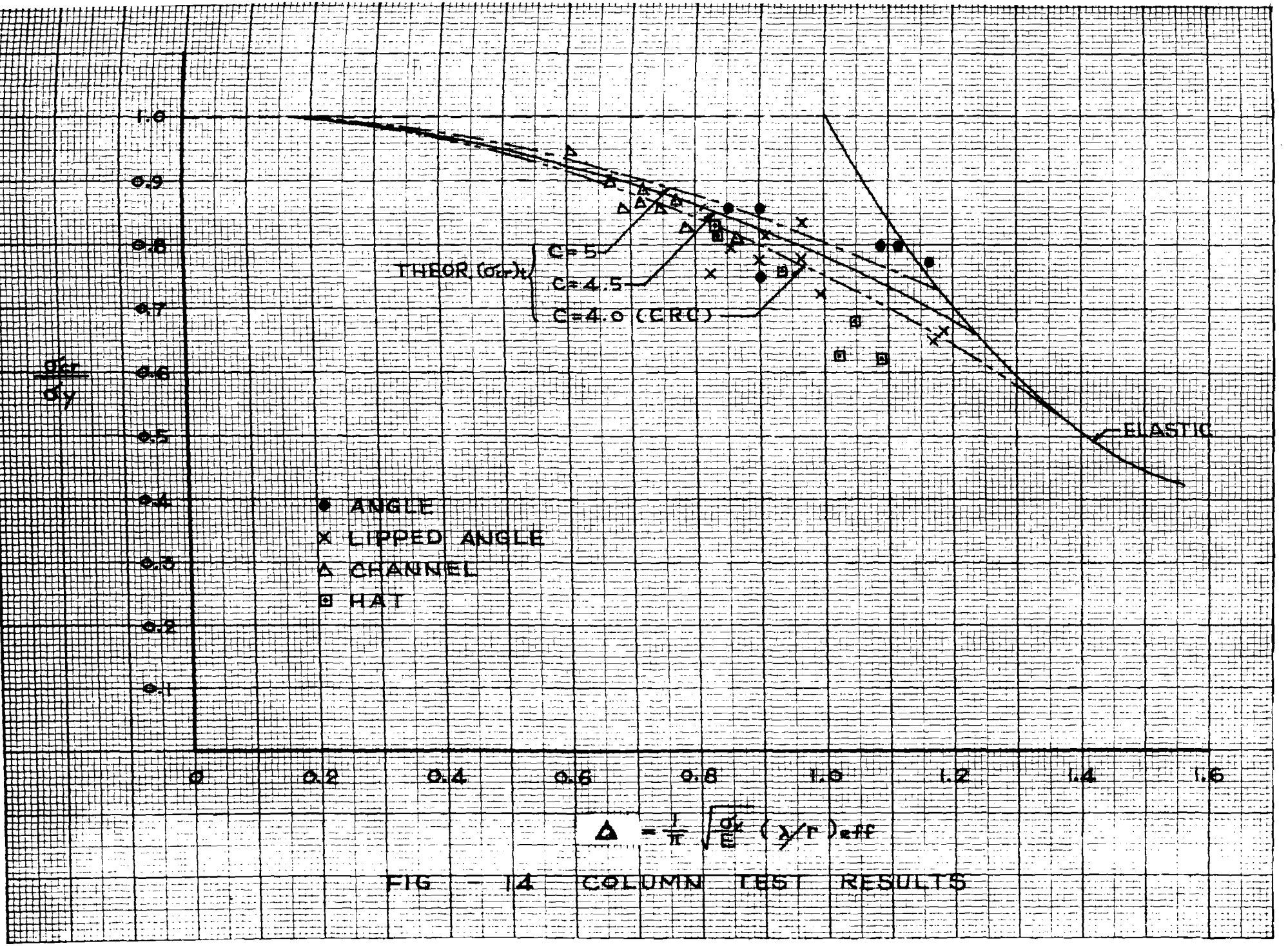

FIG - 14 COLUMN TEST RESULTS

Fig. 14

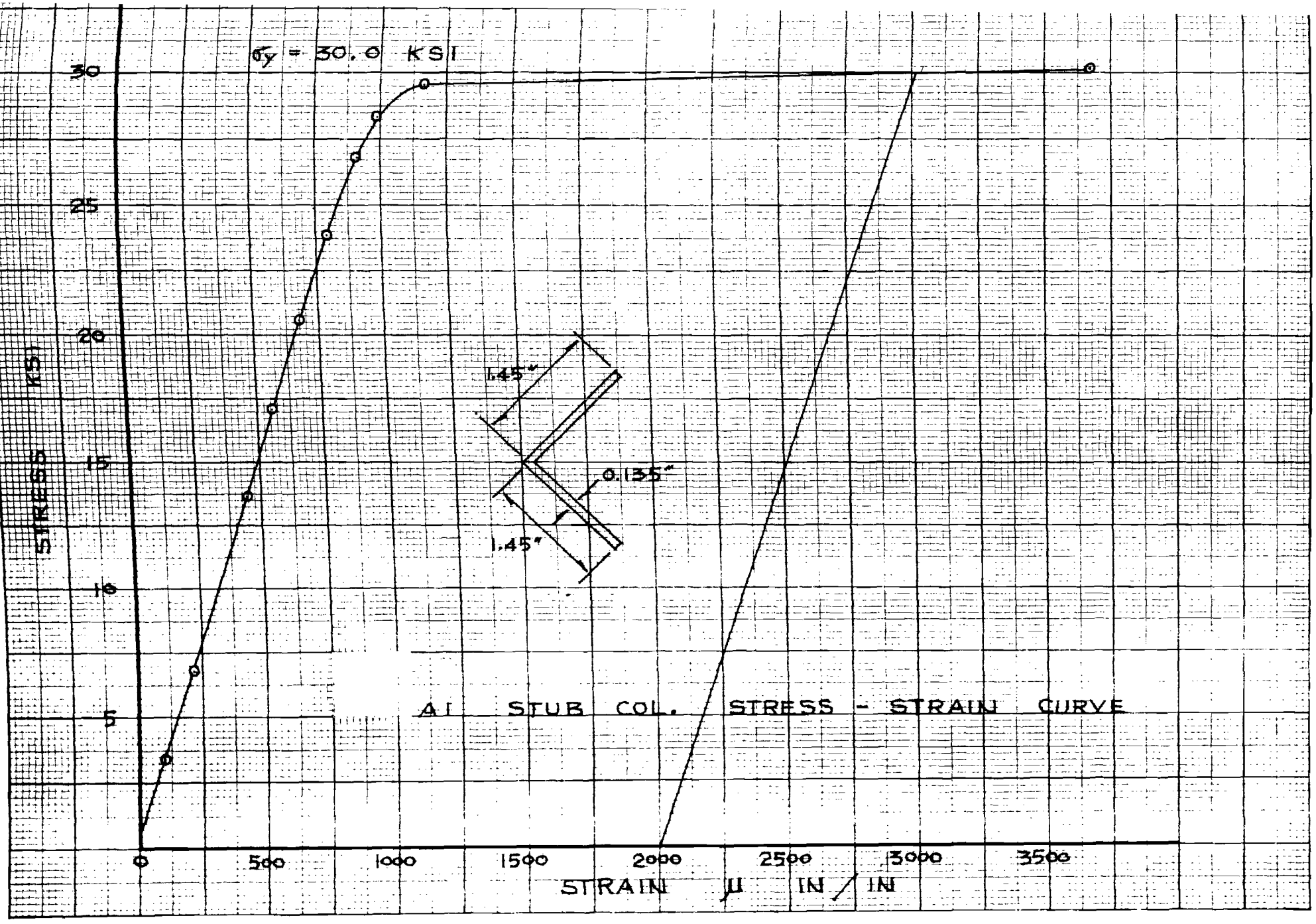

Al STUB COL. STRESS - STRAIN CURVE

Fig. 15

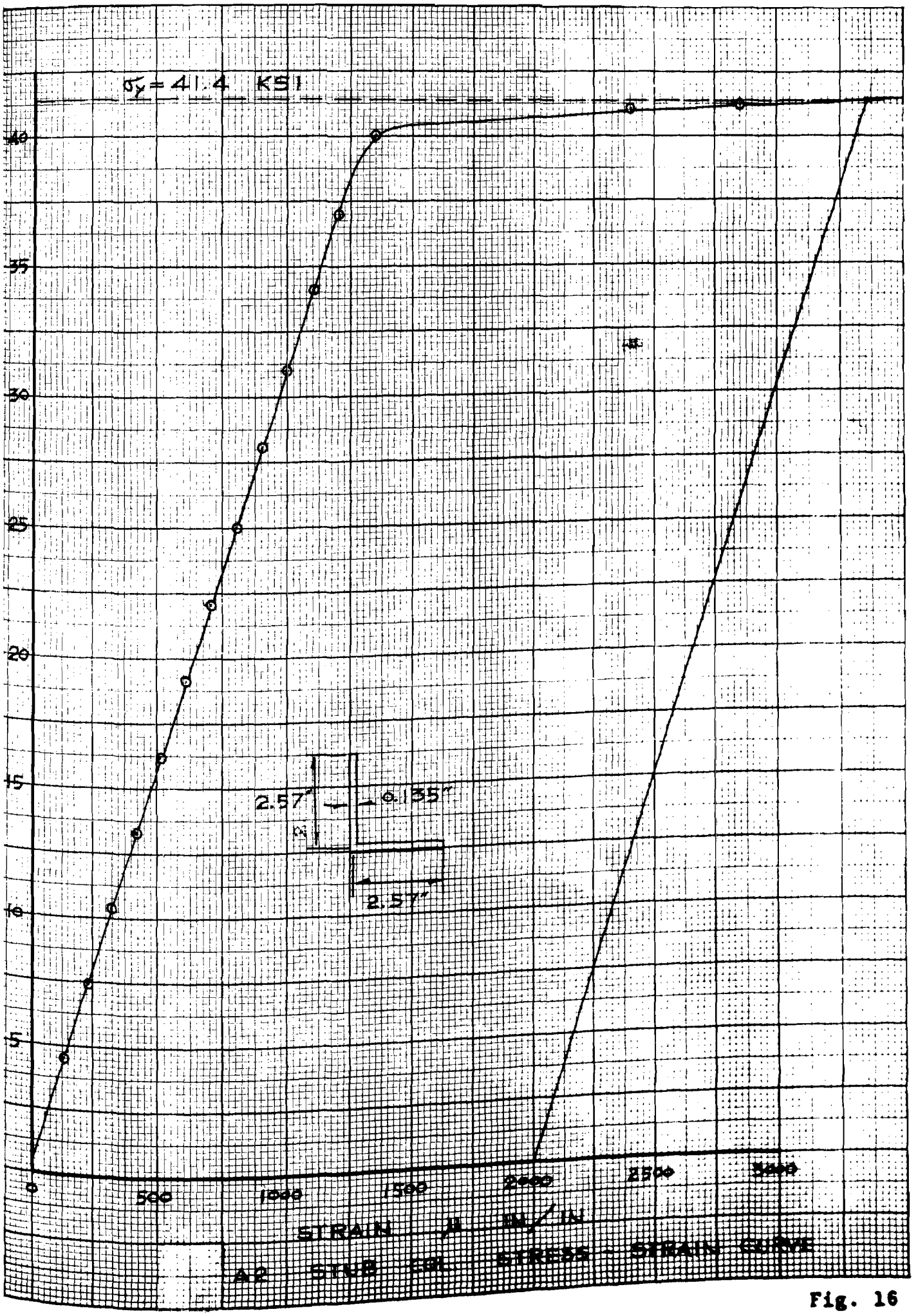
σy = 41.4 KSI
40
35
30
25
20
15
10
5
0
500
1000
1500
2000
2500
3000
2.57"
0.135"
2.57"
STRAIN μ IN/IN
A2 STUB COL. STRESS - STRAIN CURVE

Fig. 16

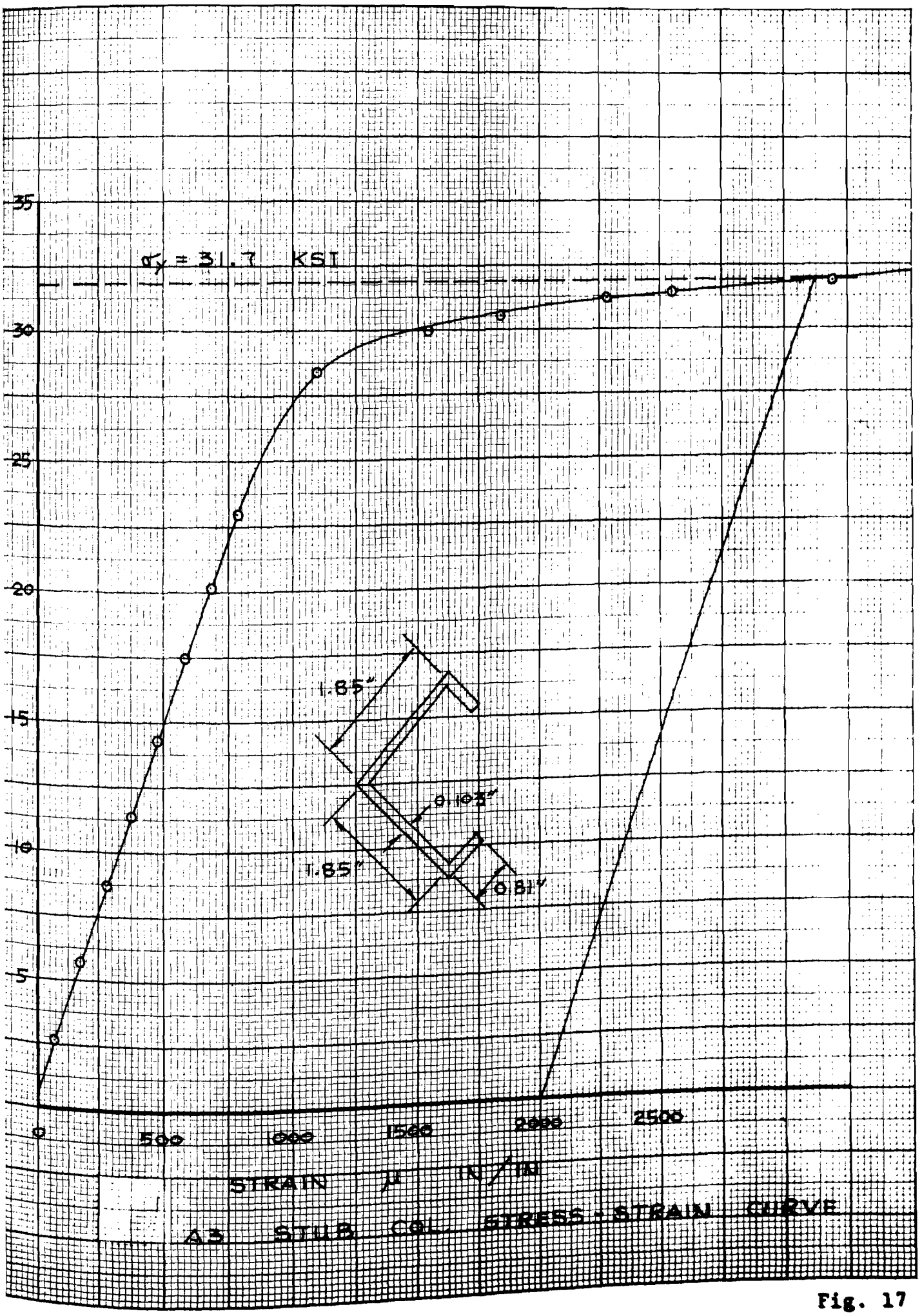

A3 STUB COL. STRESS - STRAIN CURVE

Fig. 17

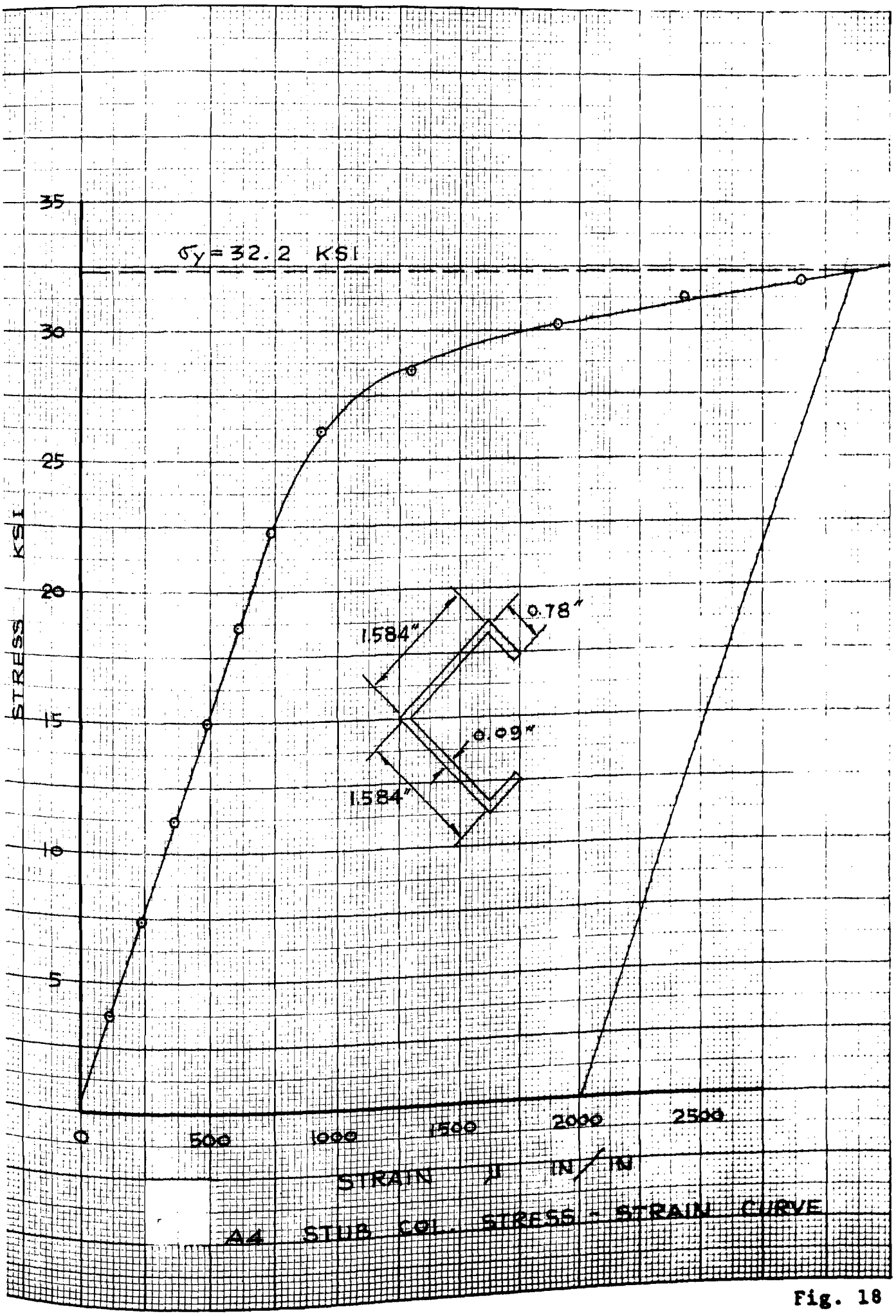

A4 STUB COL. STRESS - STRAIN CURVE

Fig. 18

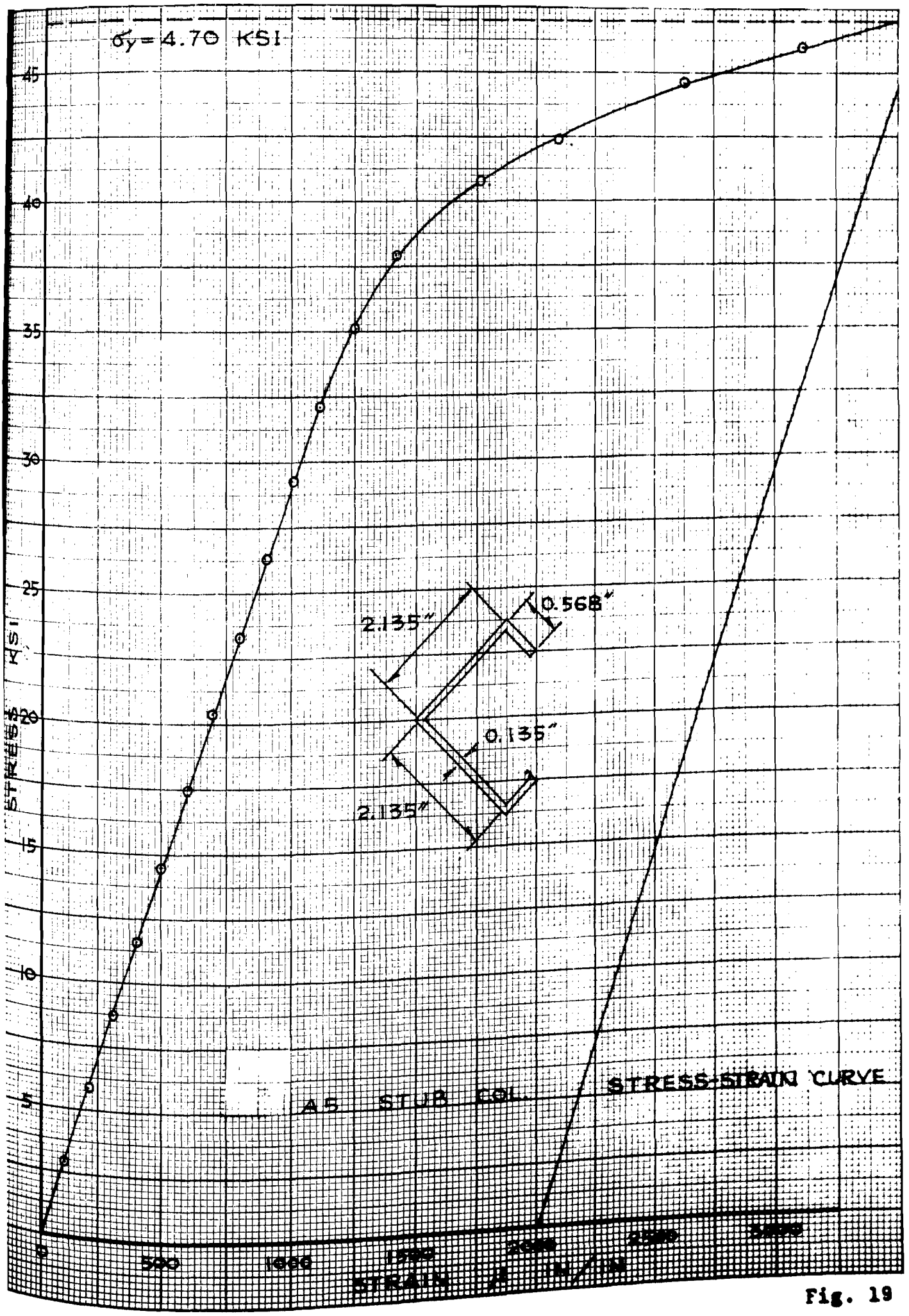
σy = 4.70 KSI
45
40
35
30
25
20
15
10
5
0
STRESS KSI
2.135"
0.568"
0.135"
2.135"
500
1000
STRAIN
A5 STUB COL. STRESS-STRAIN CURVE

Fig. 19

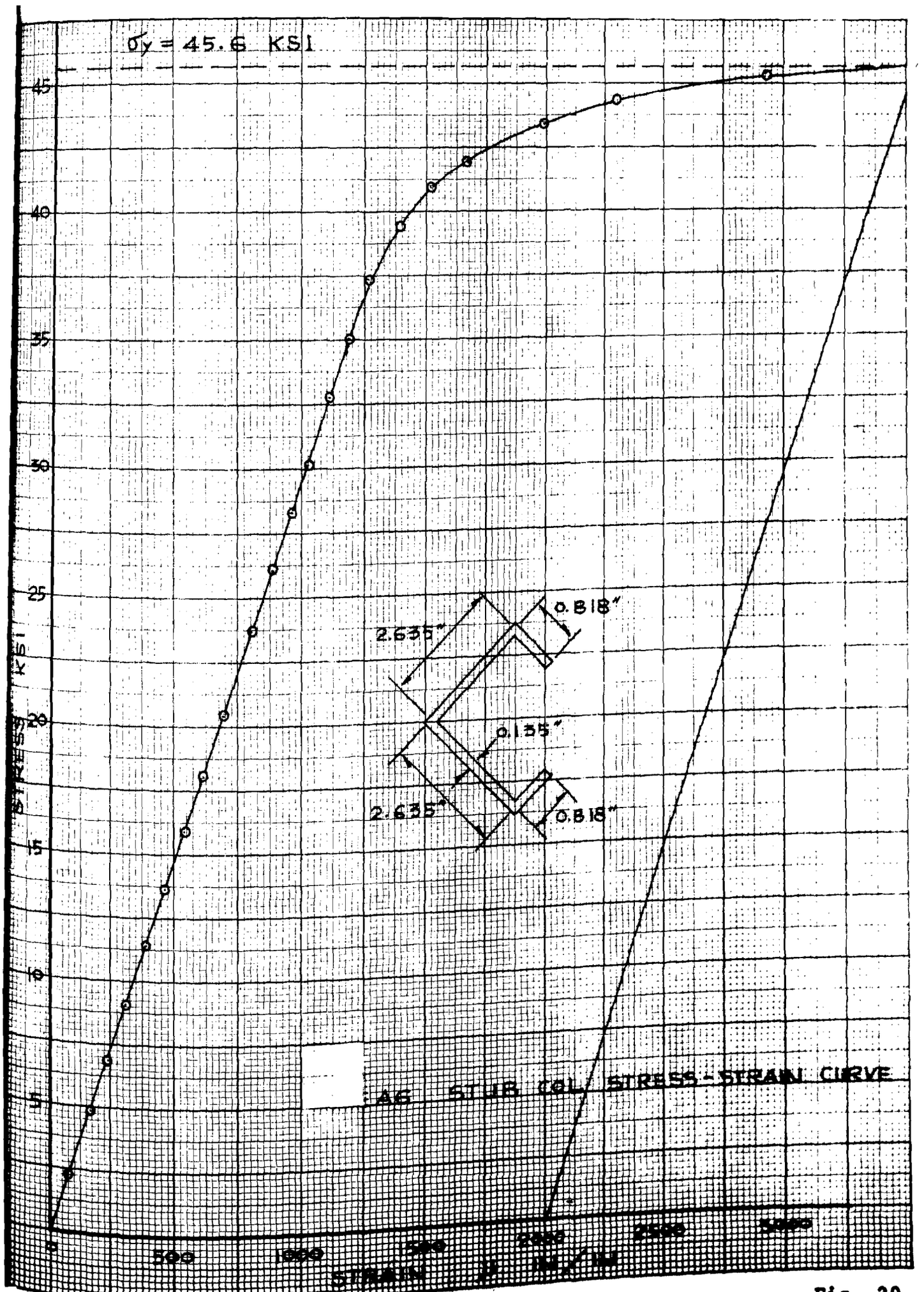
σy = 45.6 KSI
STRESS KSI
STRAIN
0.818"
2.635"
0.135"
2.635"
0.818"
AG STUB COL. STRESS-STRAIN CURVE

Fig. 20

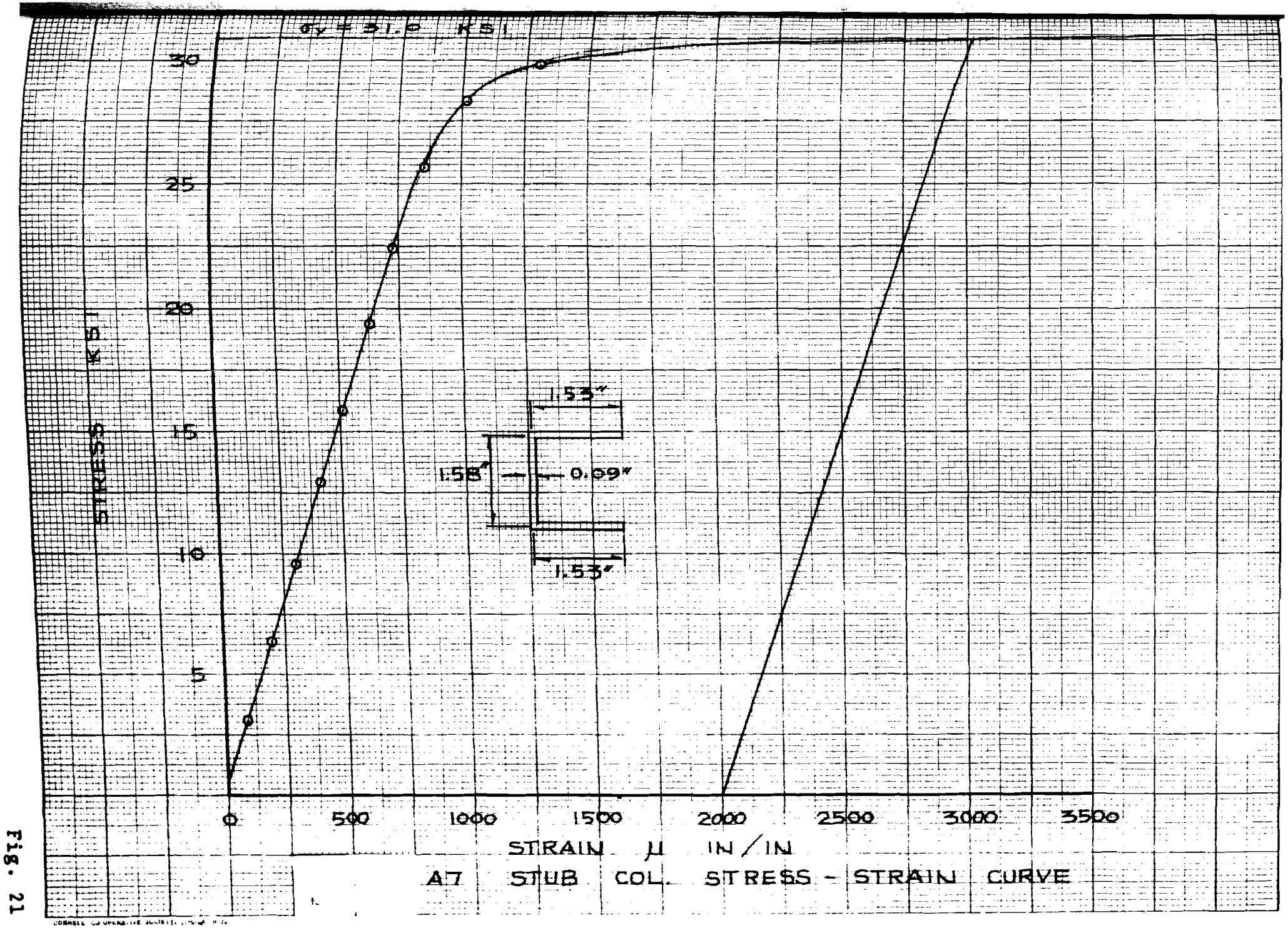

A7 STUB COL. STRESS - STRAIN CURVE

Fig. 21

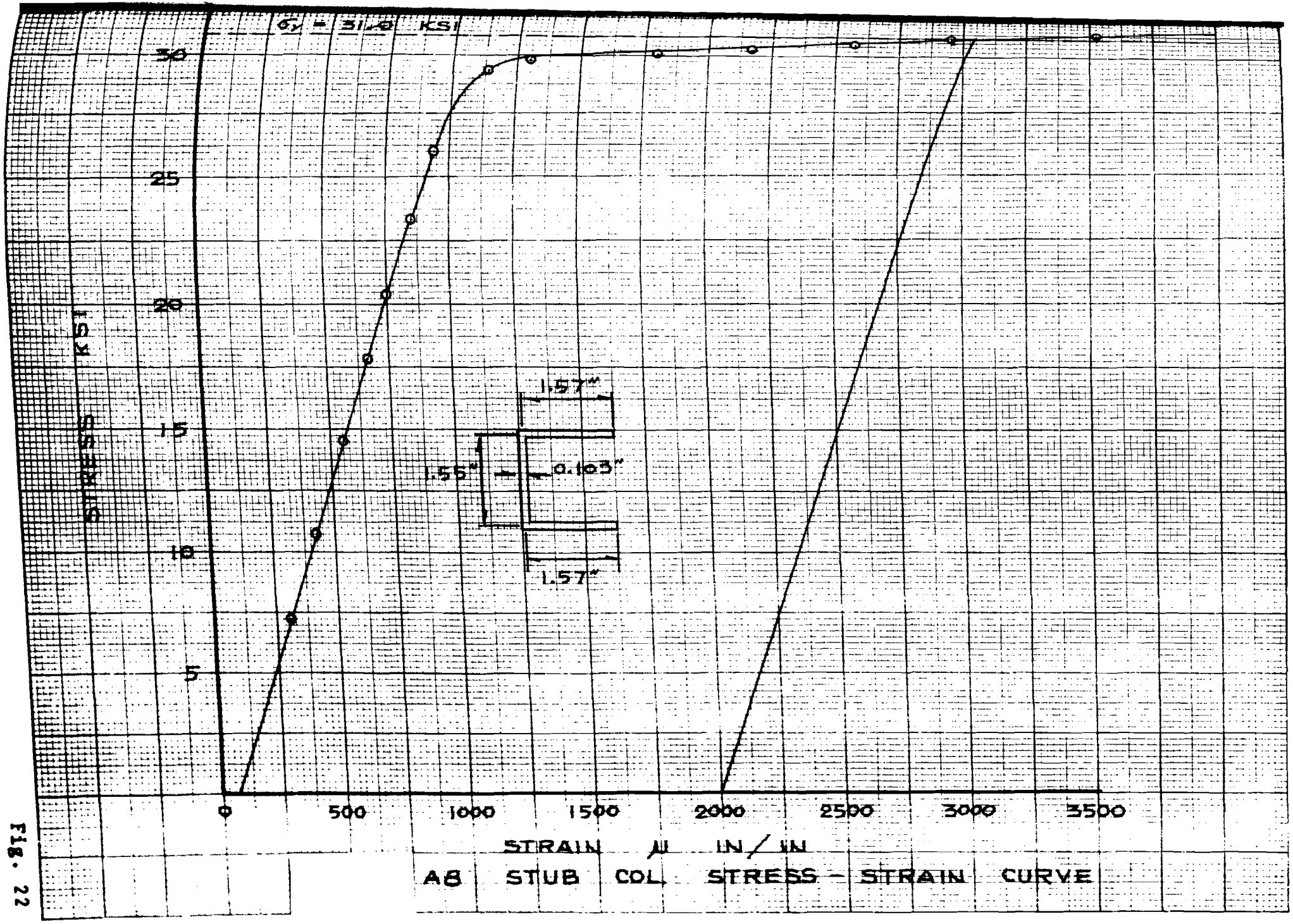

AB STUB COL. STRESS - STRAIN CURVE

Fig. 22

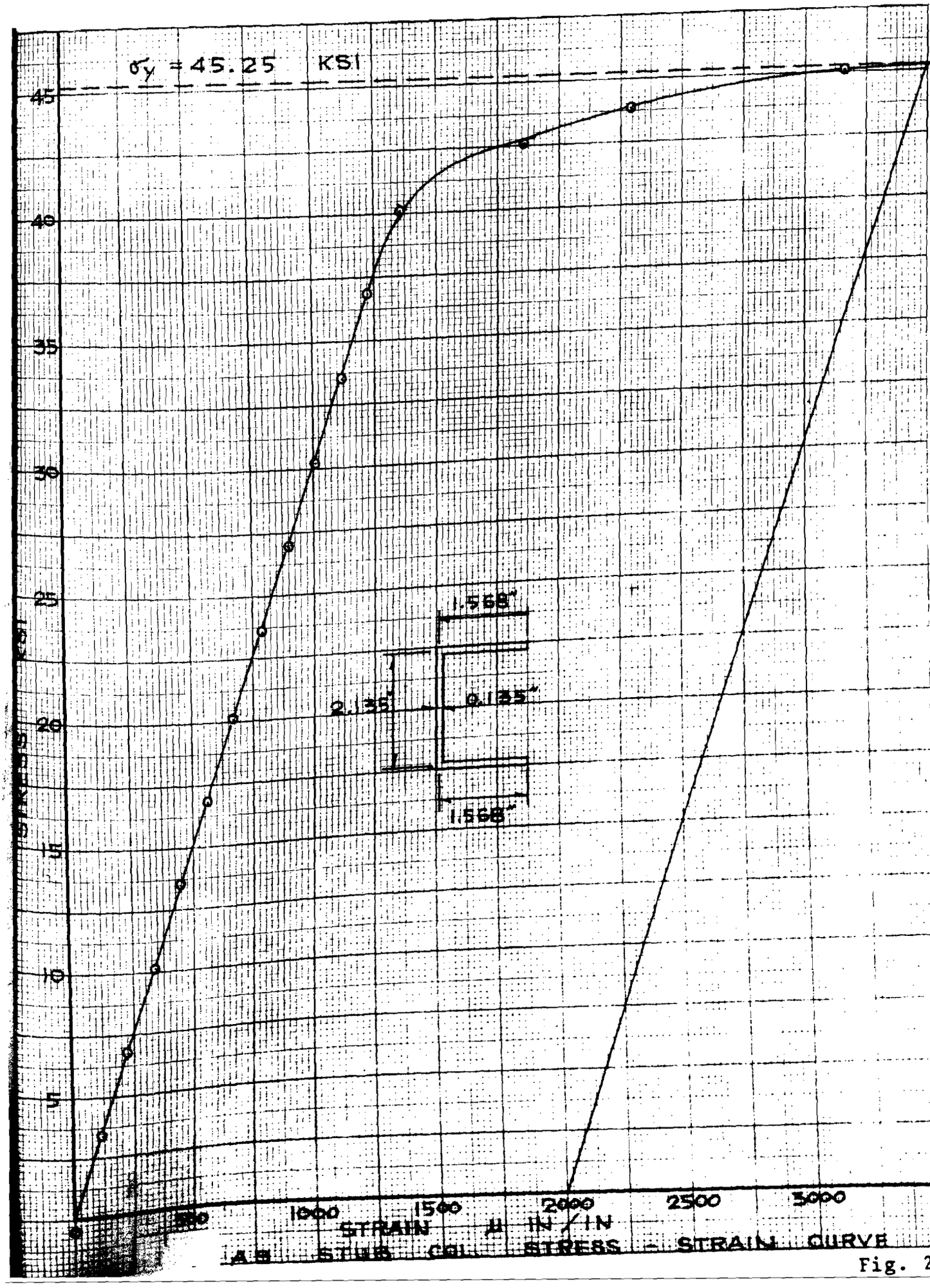
σy = 45.25 KSI
45
40
35
30
25
20
15
10
5
1.568"
2.135"
0.125"
1.568"
1000
1500
2000
2500
3000
STRAIN μ IN/IN
A36 STEEL COUPON STRESS - STRAIN CURVE

Fig. 23

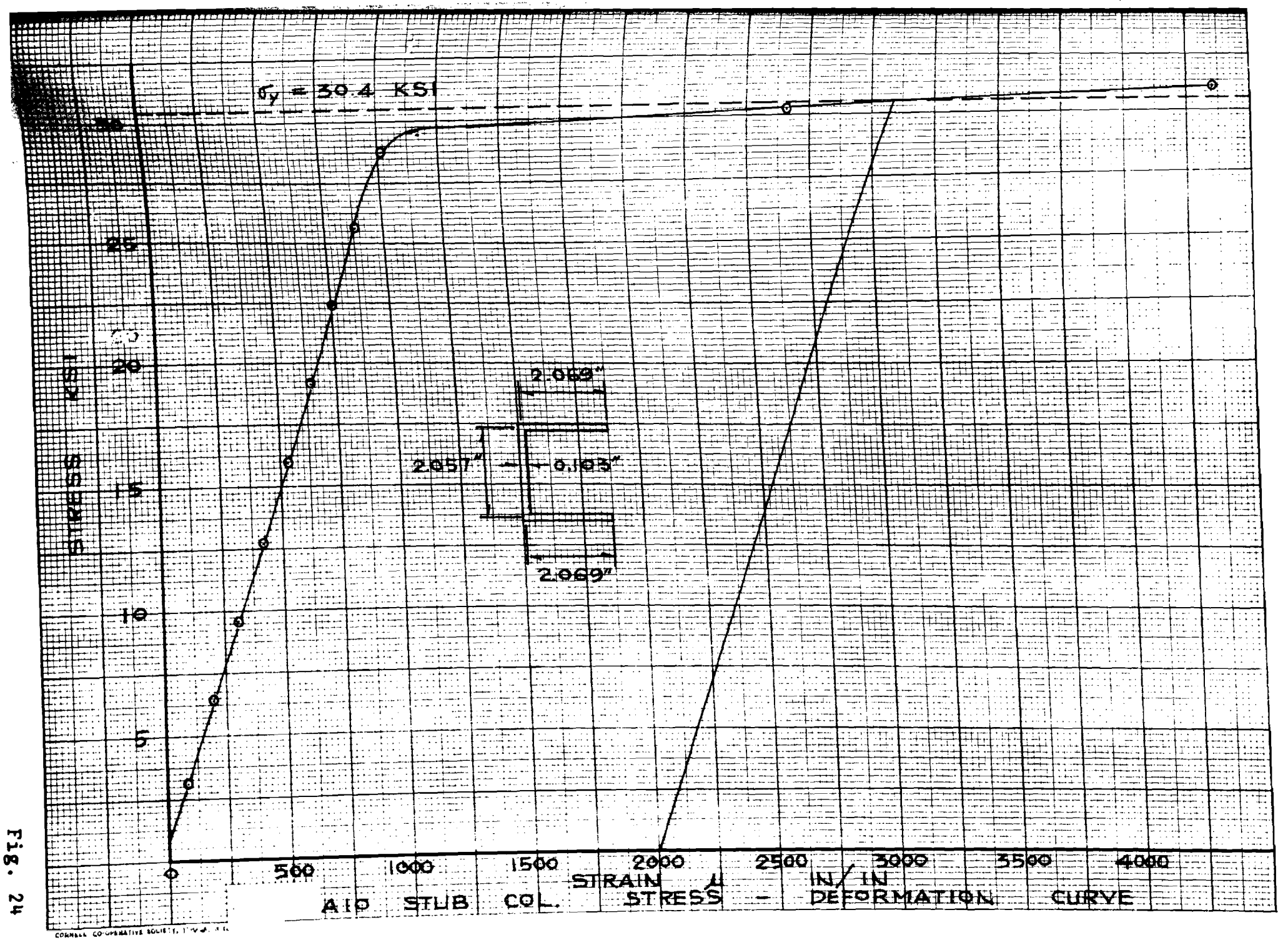
σ_y = 30.4 KSI
2.063"
2.057"
0.103"
2.069"
STRESS - KSI
0
5
10
15
20
25
500
1000
1500
2000
2500
3000
3500
4000
STRAIN μ IN/IN
AID STUB COL. STRESS - DEFORMATION CURVE

Fig. 24

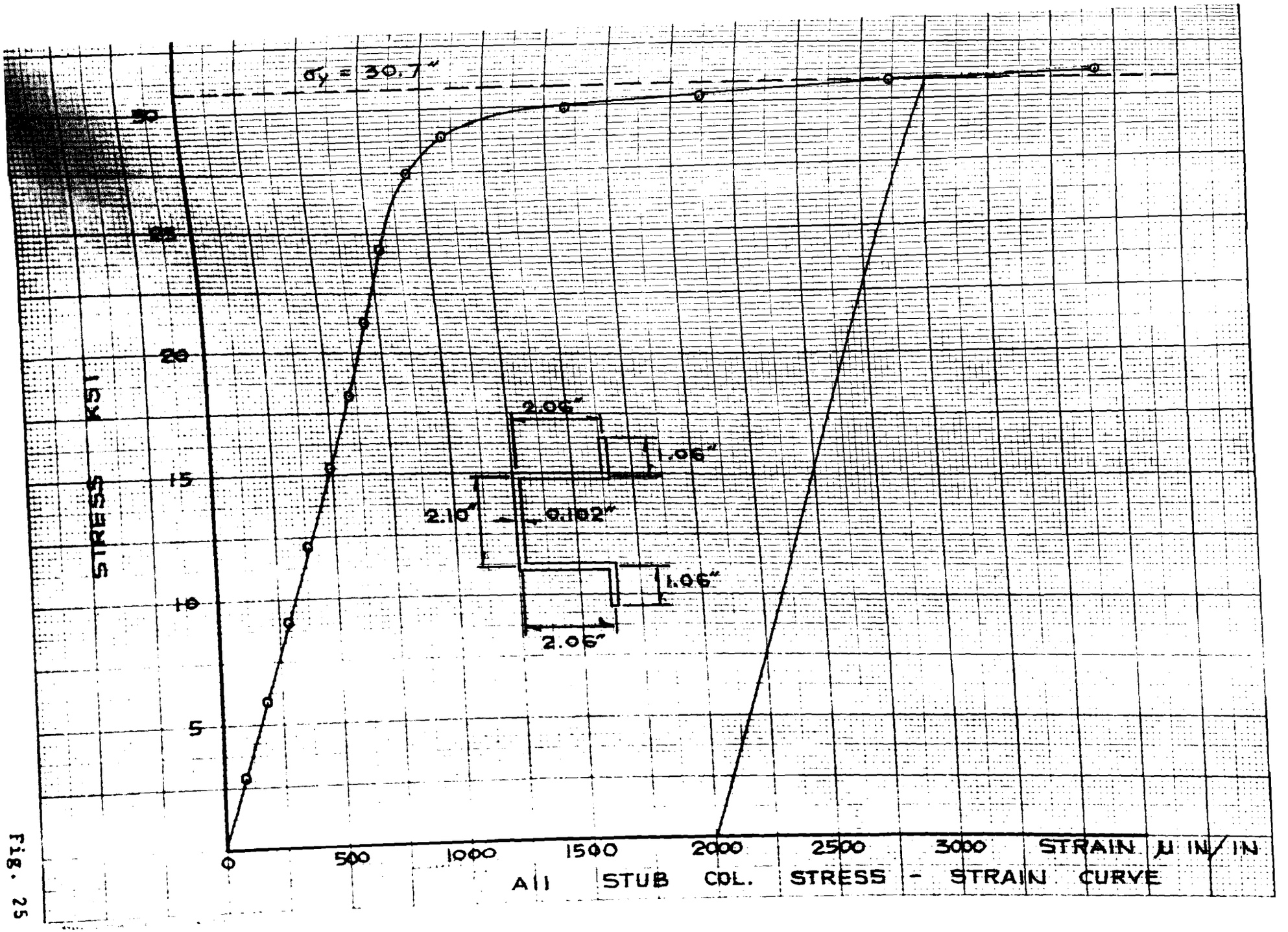

All STUB COL. STRESS - STRAIN CURVE

Fig. 25

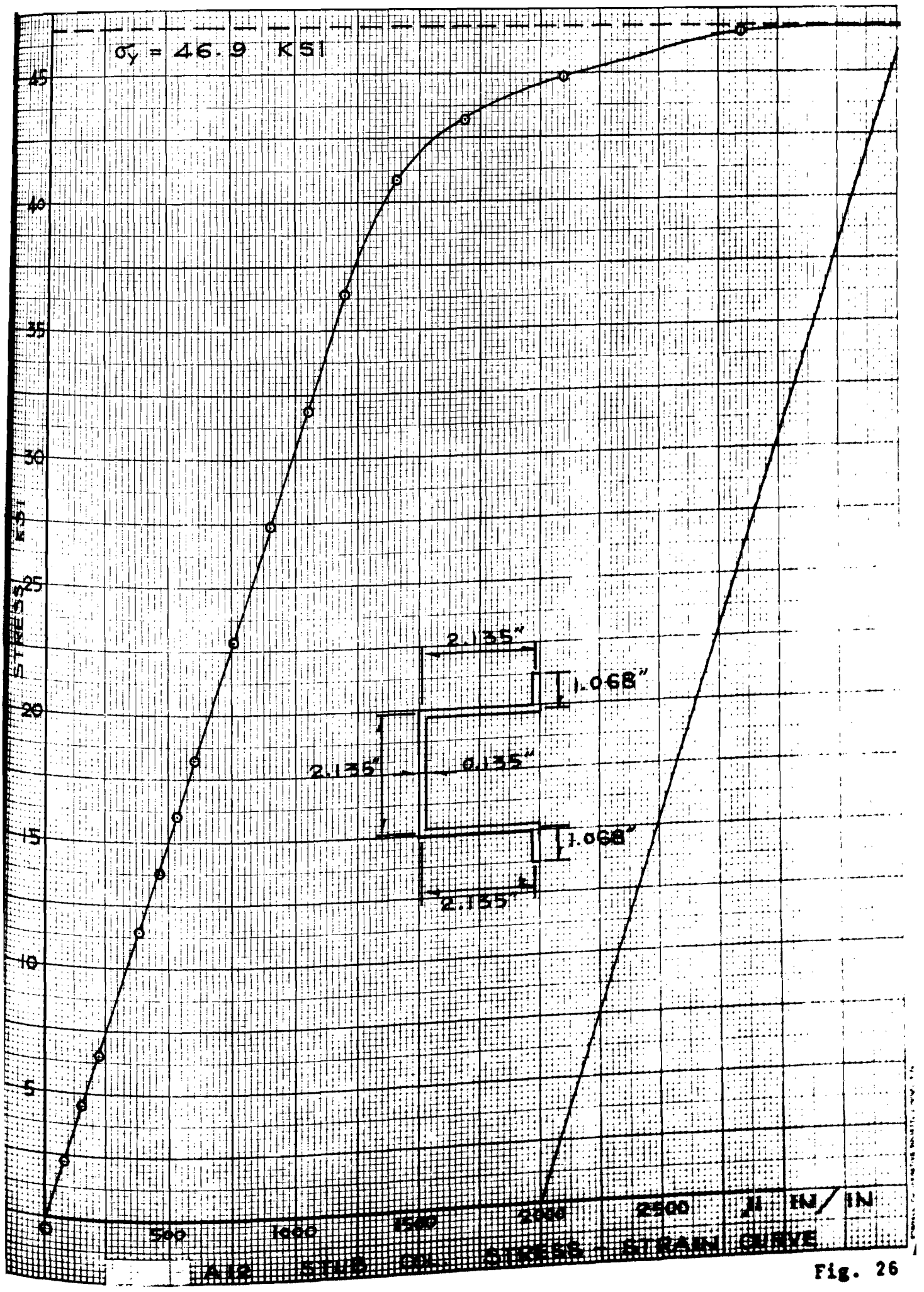
σy = 46.9 KSI
STRESS KSI
45
40
35
30
25
20
15
10
5
2.135"
1.068"
2.135"
0.135"
1.068"
2.135"
500
1000
1500
2000
2500
μ IN/IN
AIR STEEL OIL STRESS STRAIN CURVE

Fig. 26

APPENDIX B

Stress-Deformation Curves of Column Specimens

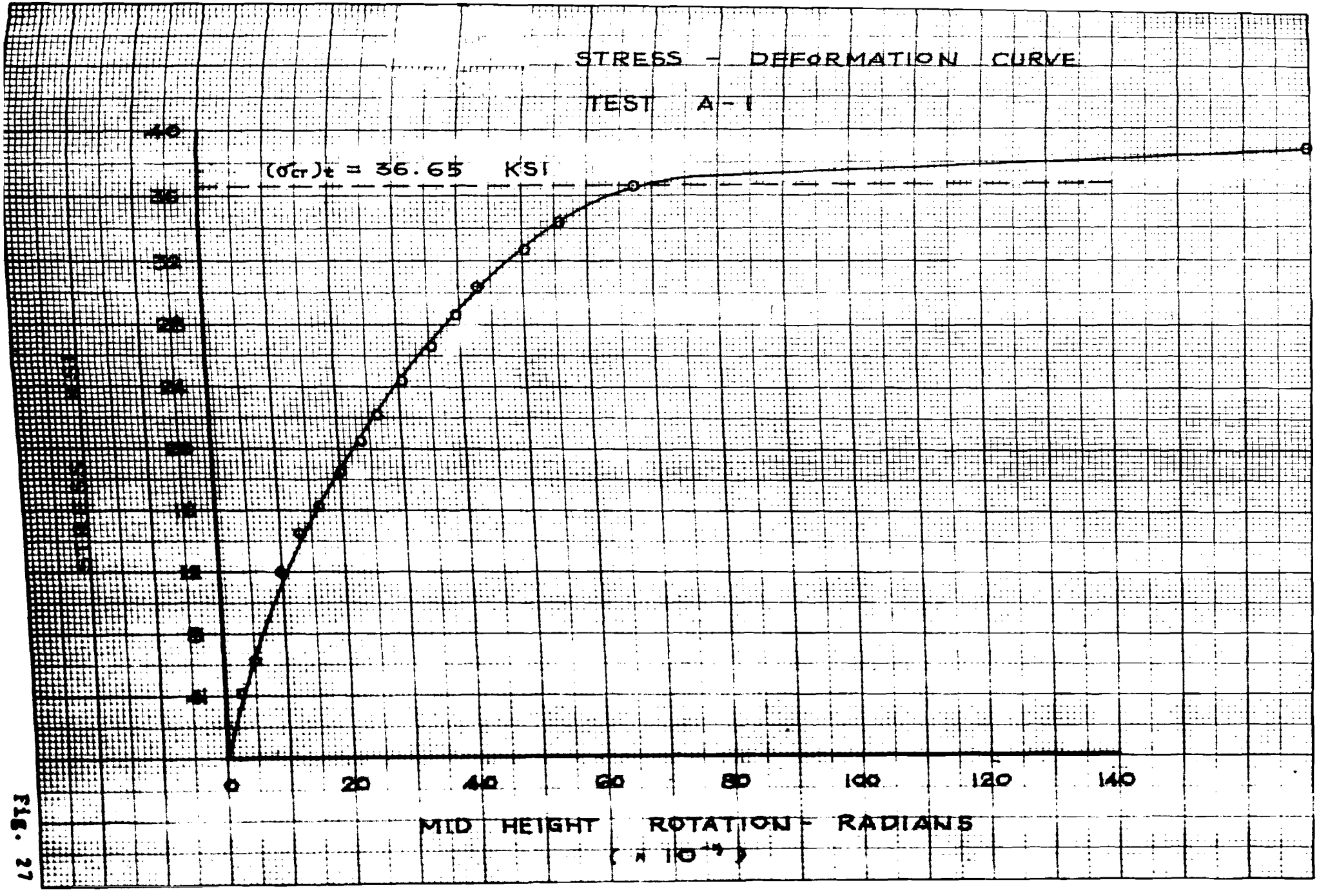
STRESS - DEFORMATION CURVE
TEST A-1
$(\sigma_{cr})_t$ = 36.65 KSI
40
36
32
28
24
20
16
12
8
4
0
0
20
40
60
80
100
120
140
MID HEIGHT ROTATION - RADIANS
(x 10^{-4})

FIG. 27

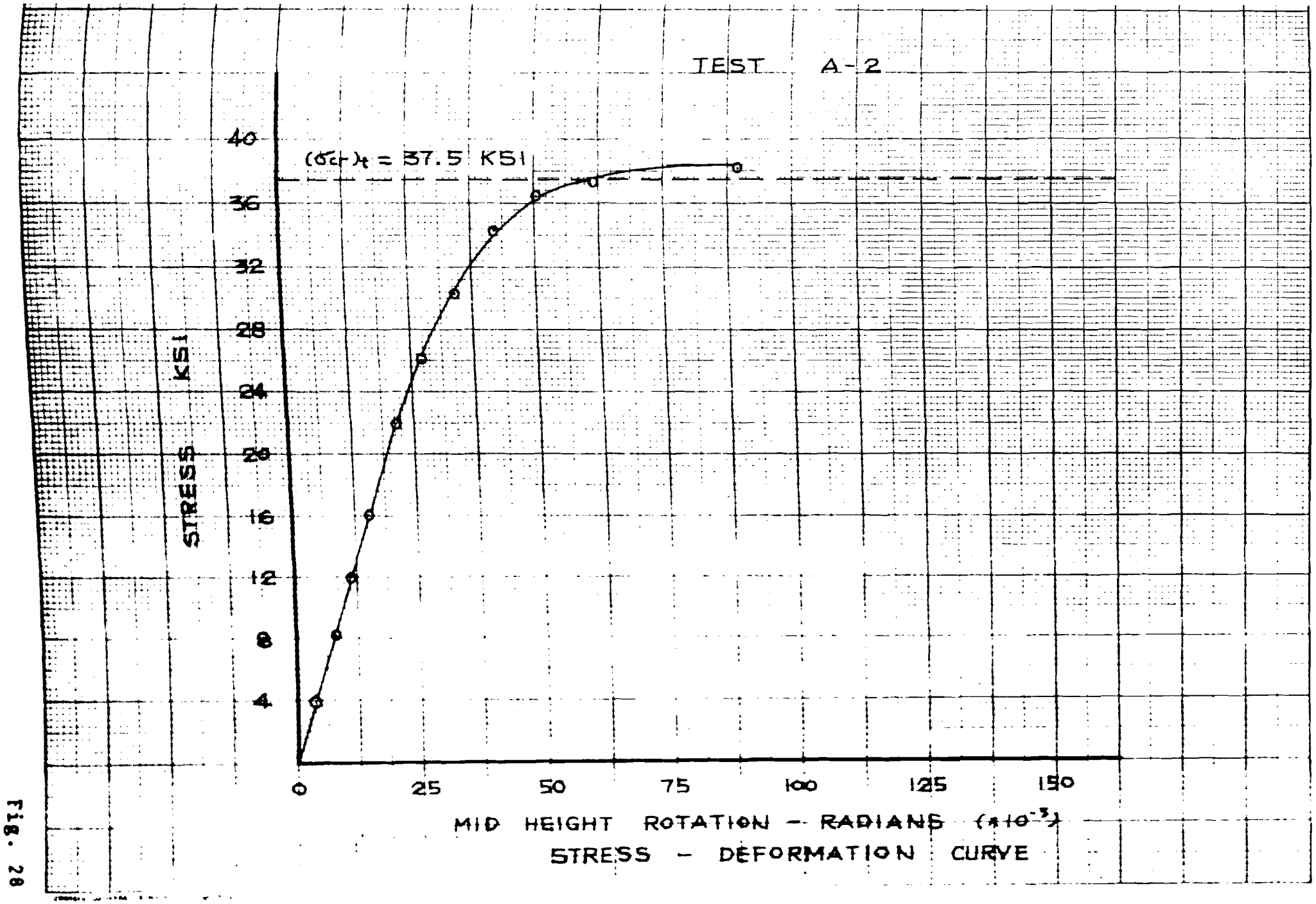

STRESS - DEFORMATION CURVE

Fig. 20

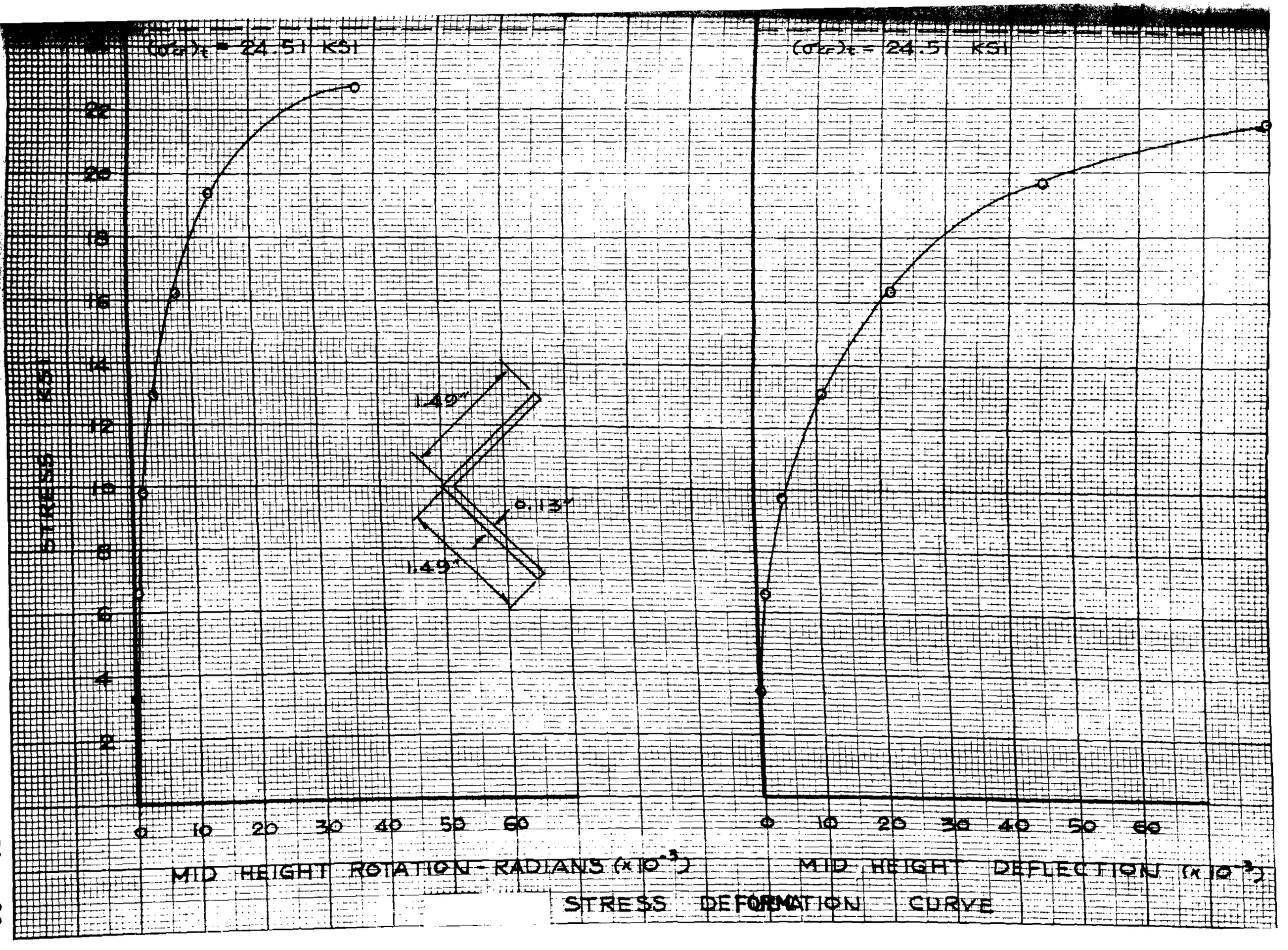

STRESS DEFORMATION CURVE

Fig. 29

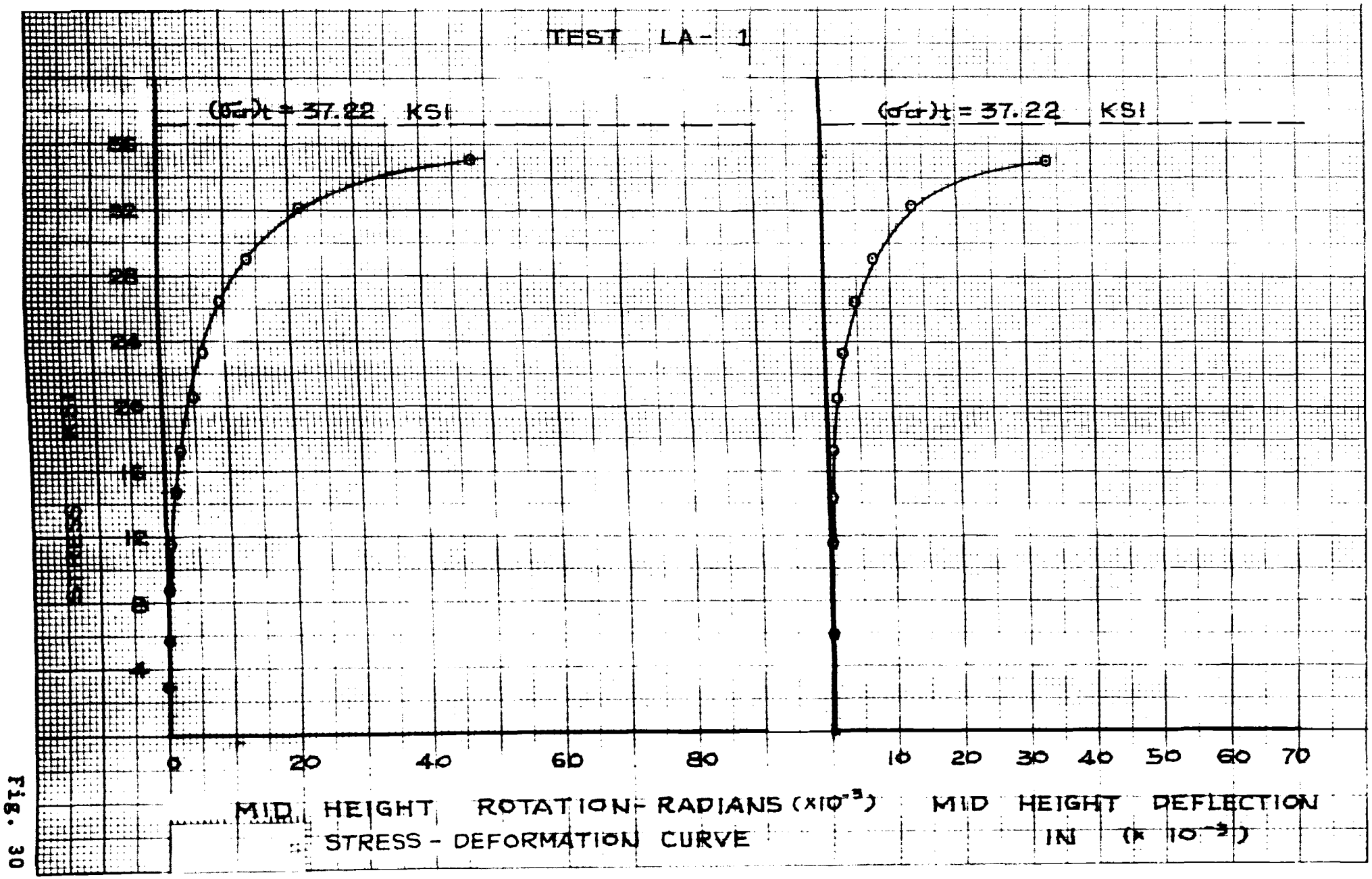

STRESS - DEFORMATION CURVE

Fig. 30

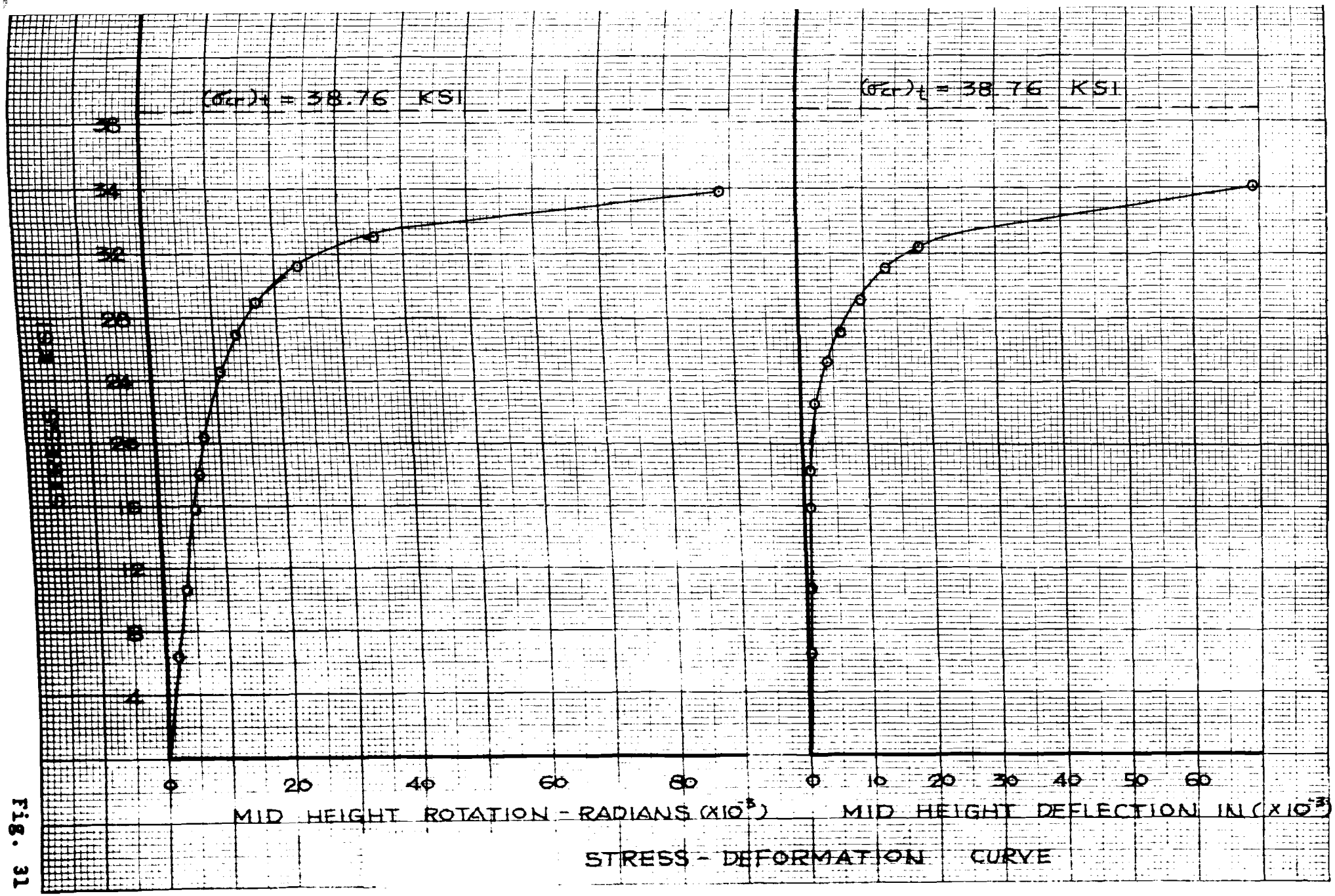

STRESS - DEFORMATION CURVE

Fig. 31

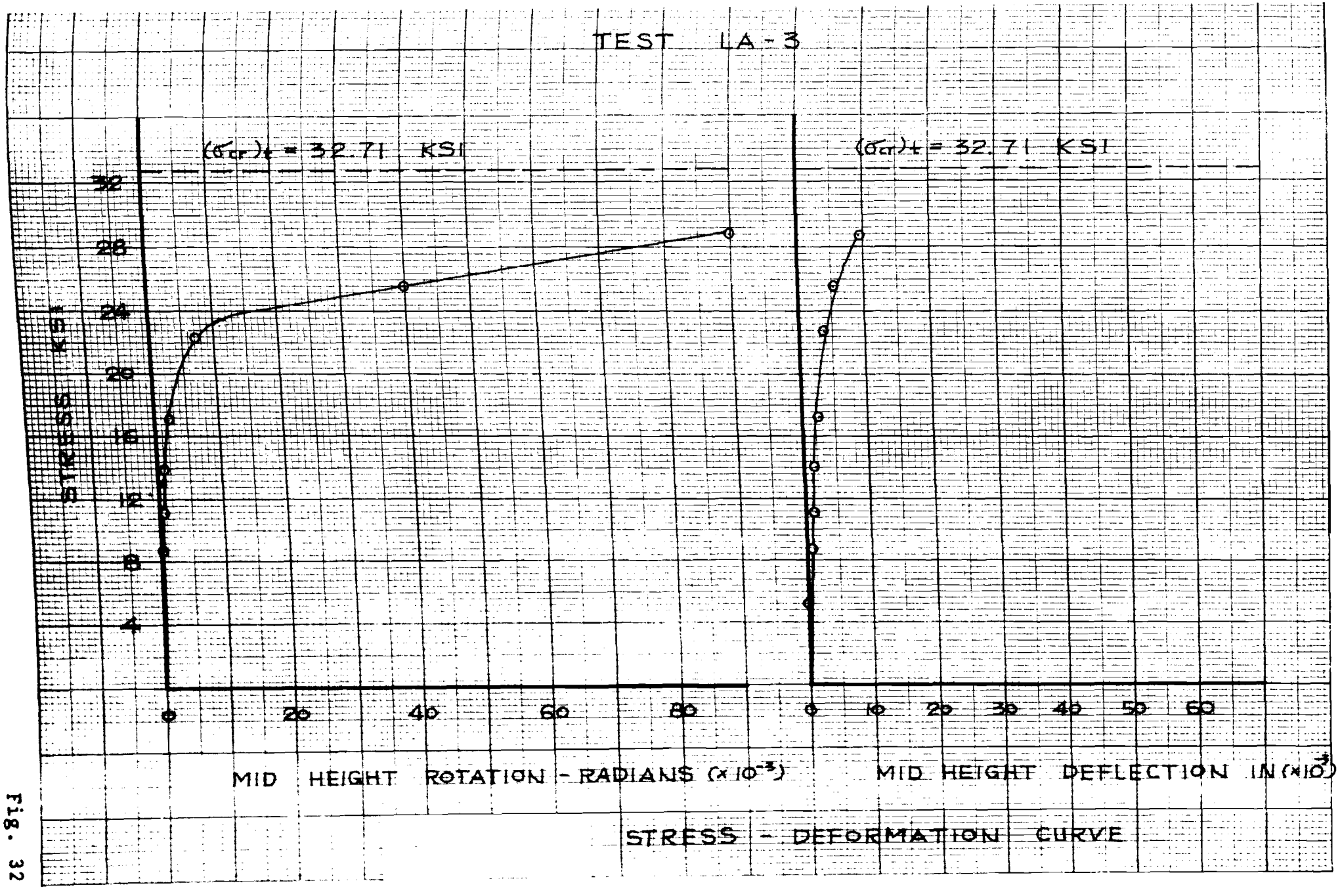

STRESS - DEFORMATION CURVE

Fig. 32

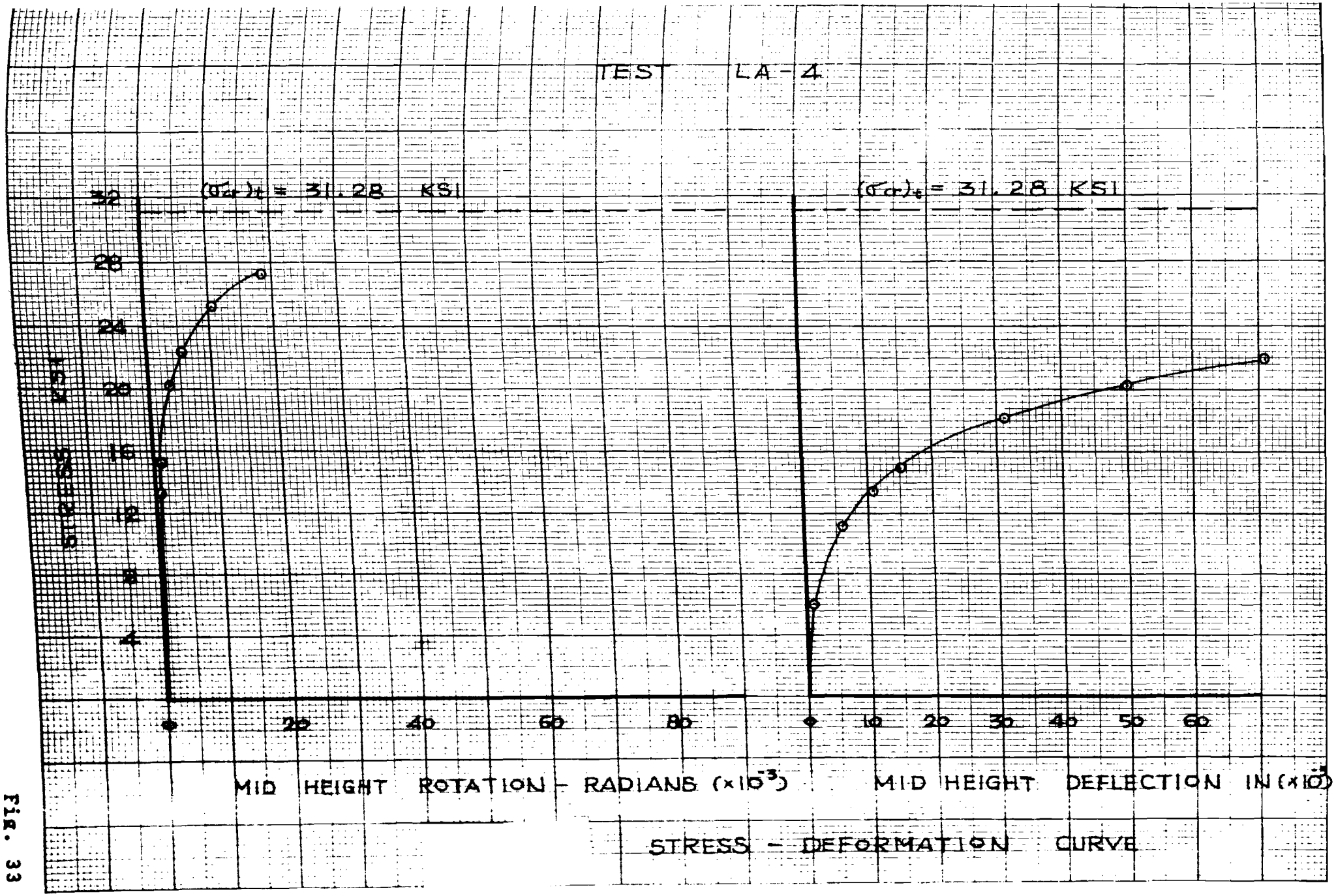

STRESS - DEFORMATION CURVE

Fig. 33

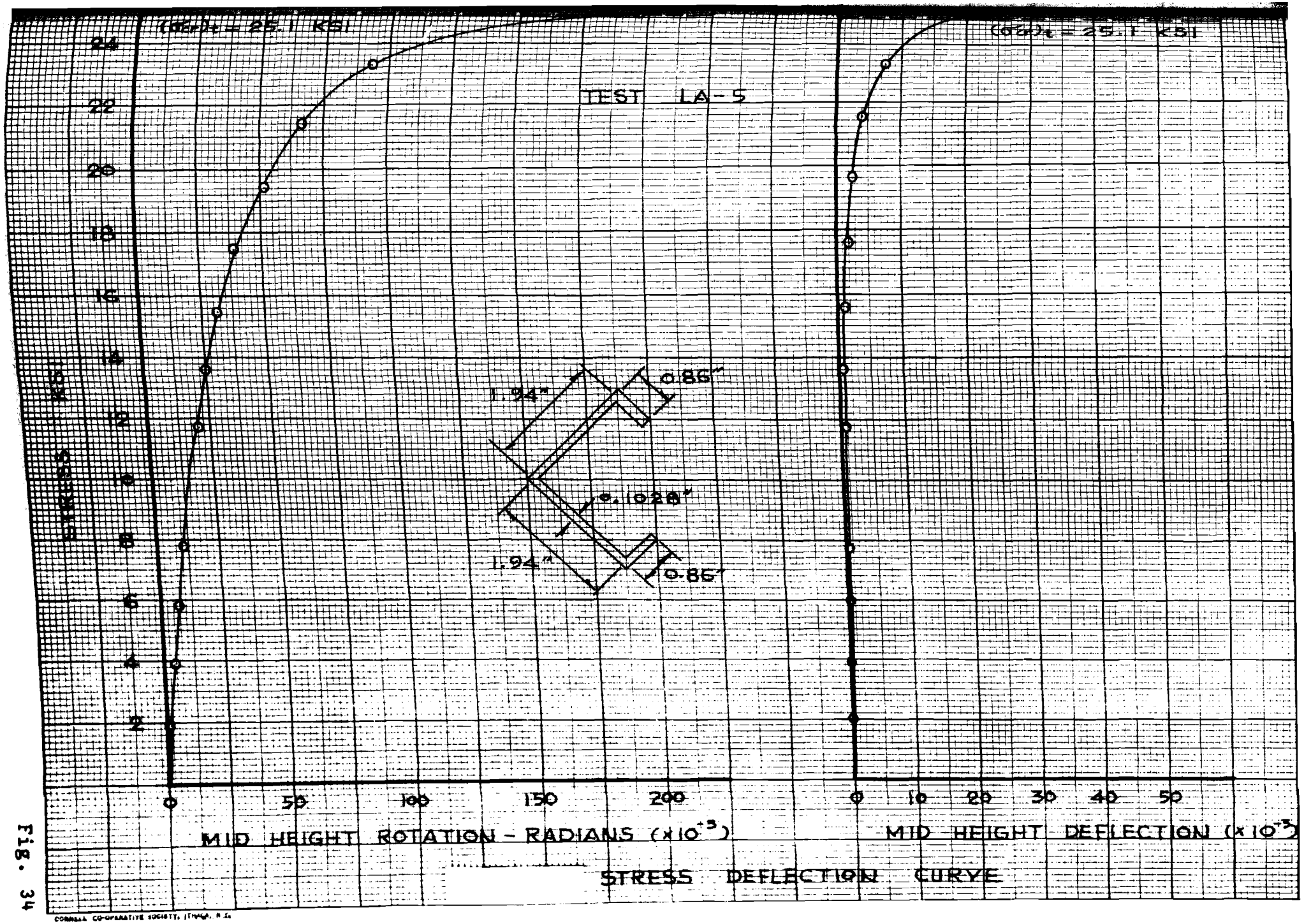

STRESS DEFLECTION CURVE

Fig. 34

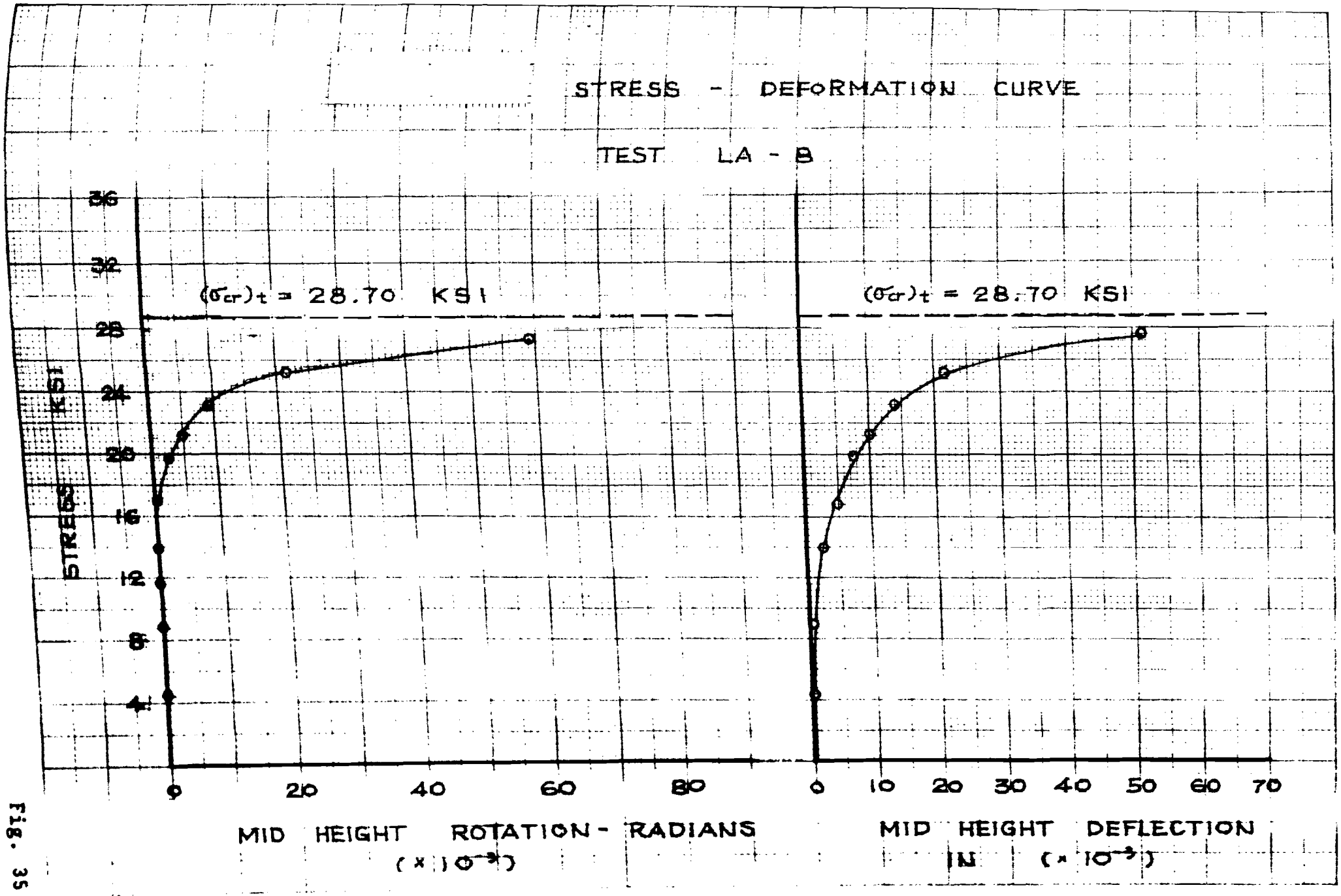
STRESS - DEFORMATION CURVE
TEST LA - B
$(\sigma_{cr})_t$ = 28.70 KSI
$(\sigma_{cr})_t$ = 28.70 KSI
STRESS KSI
36
32
28
24
20
16
12
8
4
0
20
40
60
80
0
10
20
30
40
50
60
70
MID HEIGHT ROTATION - RADIANS ($\times 10^{-3}$)
MID HEIGHT DEFLECTION IN ($\times 10^{-3}$)

Fig. 35

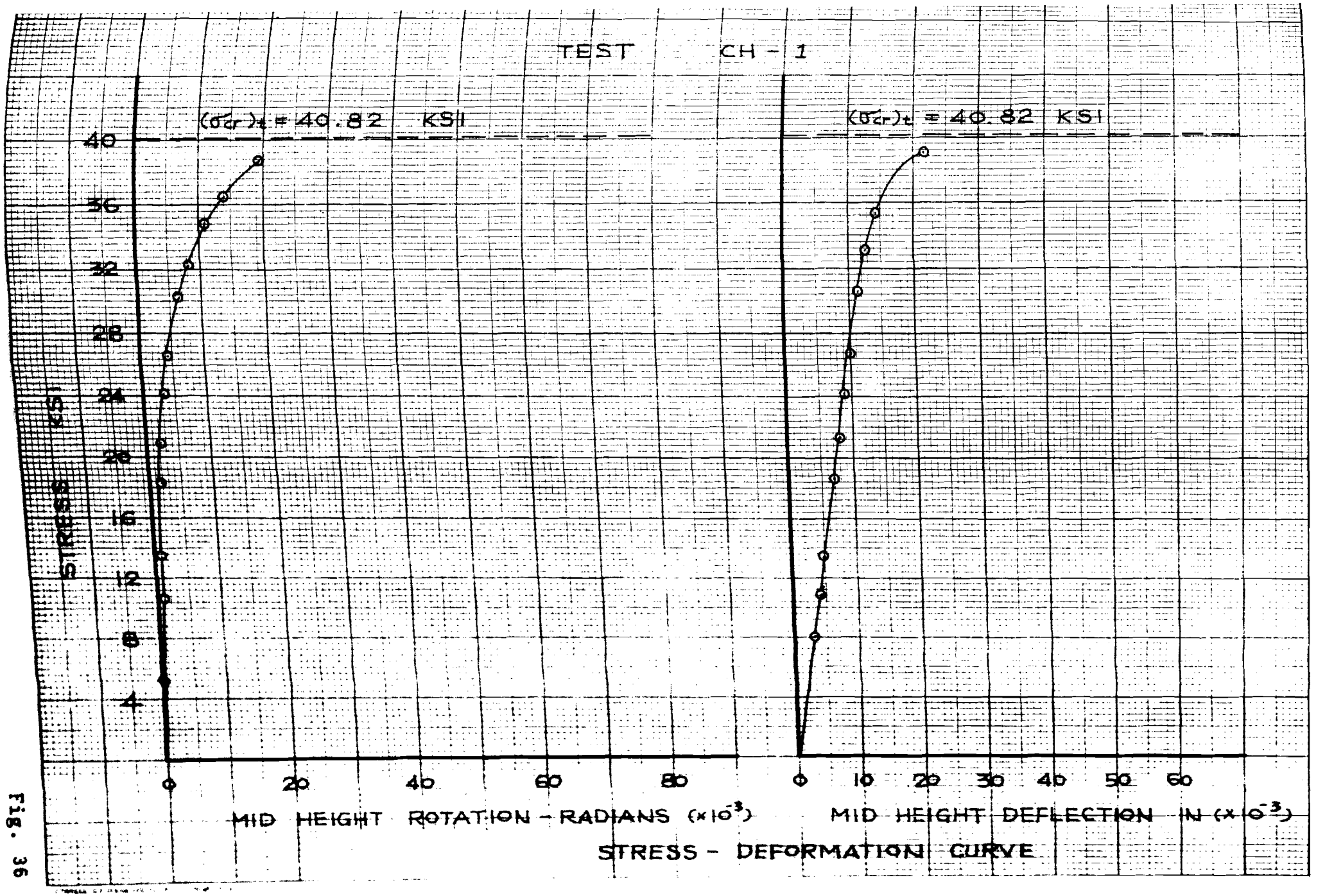

STRESS - DEFORMATION CURVE

Fig. 36

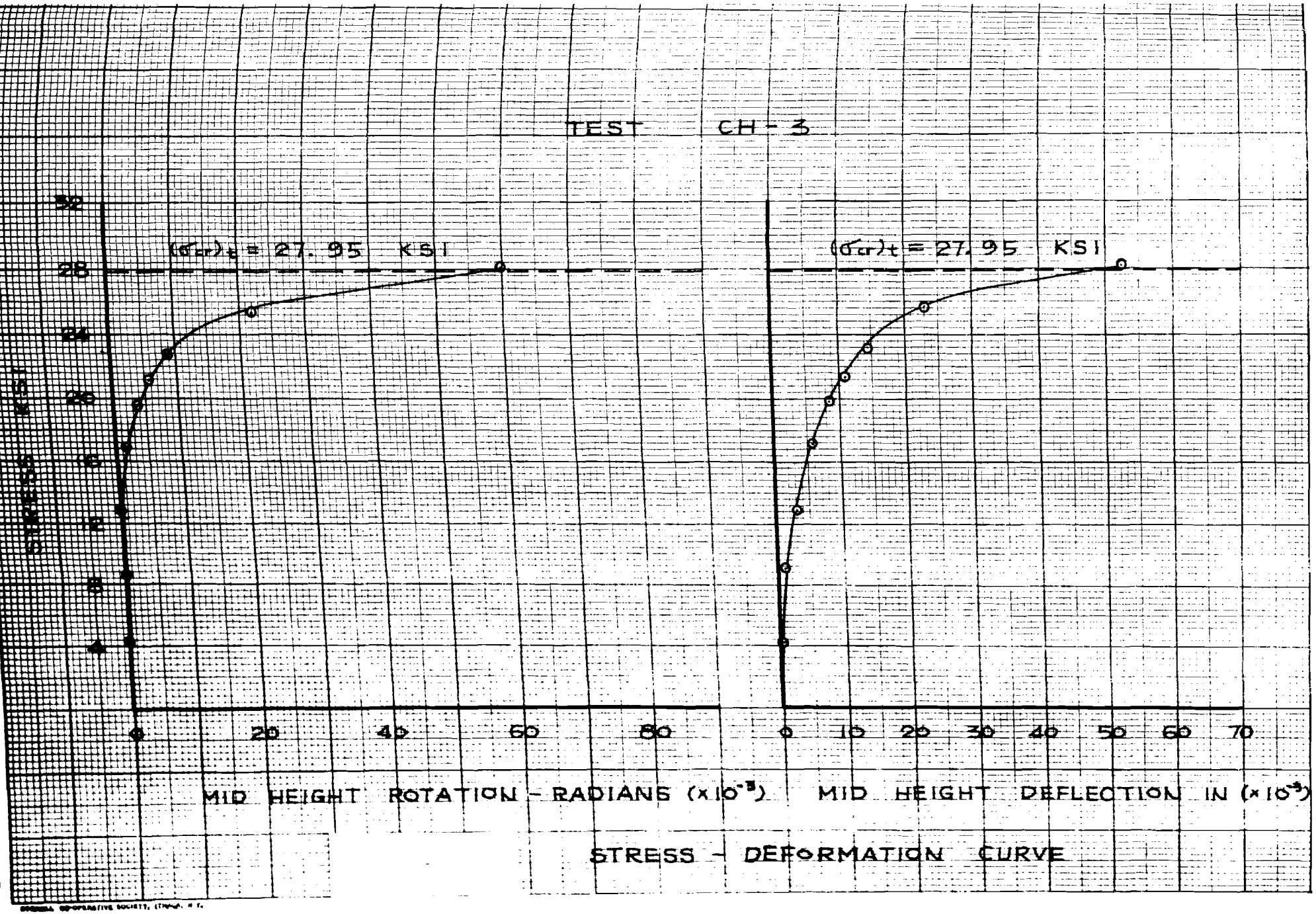

STRESS - DEFORMATION CURVE

Fig. 37

TEST - CH4
$(\sigma_{cr})_t$ = 25.98 KSI
$(\sigma_{cr})_t$ = 25.98 KSI
MID HEIGHT ROTATION - RADIANS ($\times 10^{-3}$)
MID HEIGHT DEFLECTION IN (.01")
STRESS - DEFORMATION CURVE

Fig. 38

STRESS - DEFLECTION CURVE
MID HEIGHT ROTATION - RADIANS (θ)
MID HEIGHT DEFLECTION INCHES
STRESS KSI
TEST CH-5
(σ1)1 = 26.27 KSI
(σ1)4 = 26.27 KSI

Fig. 39

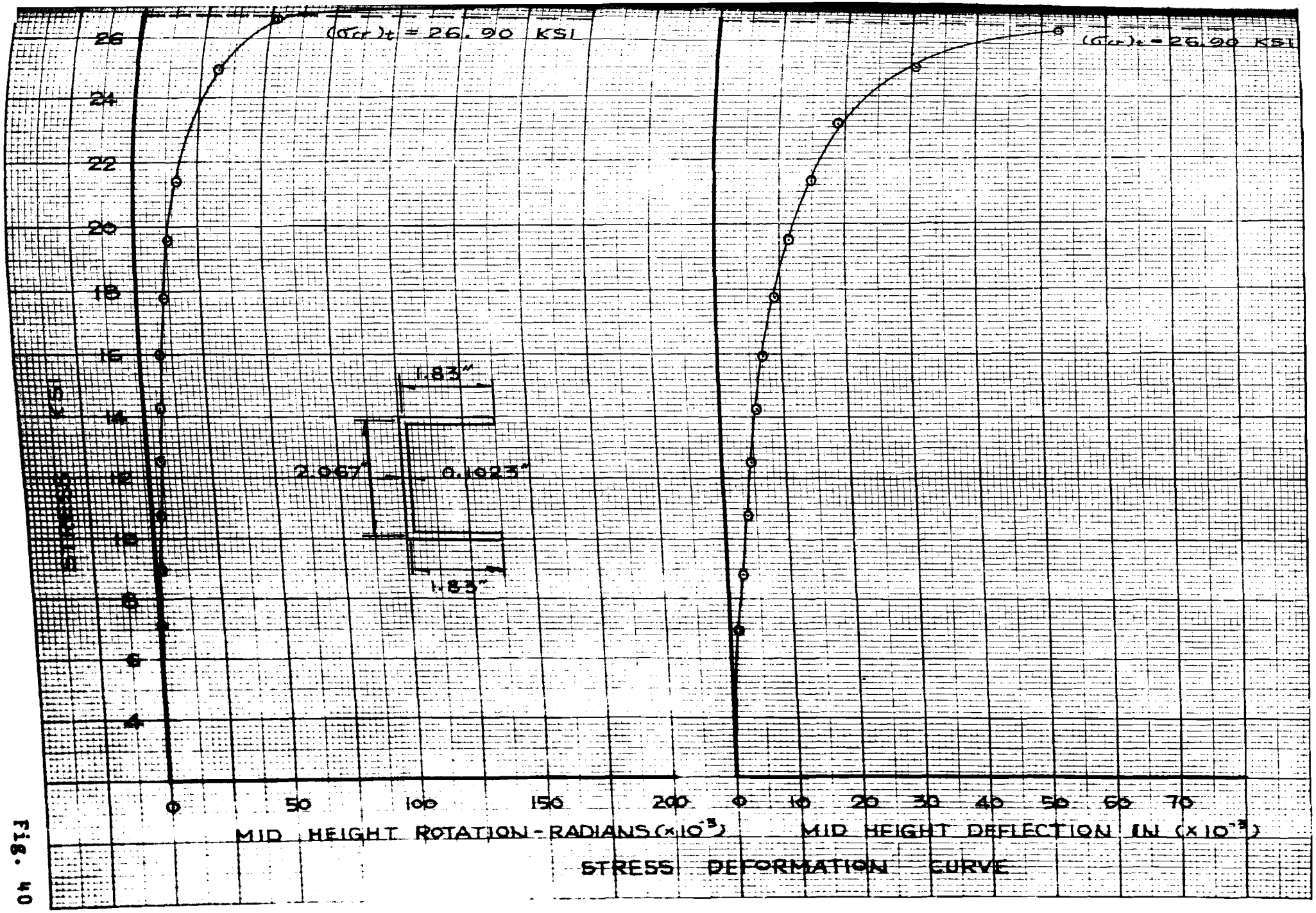
$(\sigma_{cr})_t$ = 26.90 KSI
$(\sigma_{cr})_t$ = 26.90 KSI
26
24
22
20
18
16
14
12
10
8
6
4
1.83"
2.067"
0.1023"
1.83"
0
50
100
150
200
0
10
20
30
40
50
60
70
MID HEIGHT ROTATION - RADIANS (×10⁻³)
MID HEIGHT DEFLECTION IN (×10⁻³)
STRESS DEFORMATION CURVE

Fig. 40

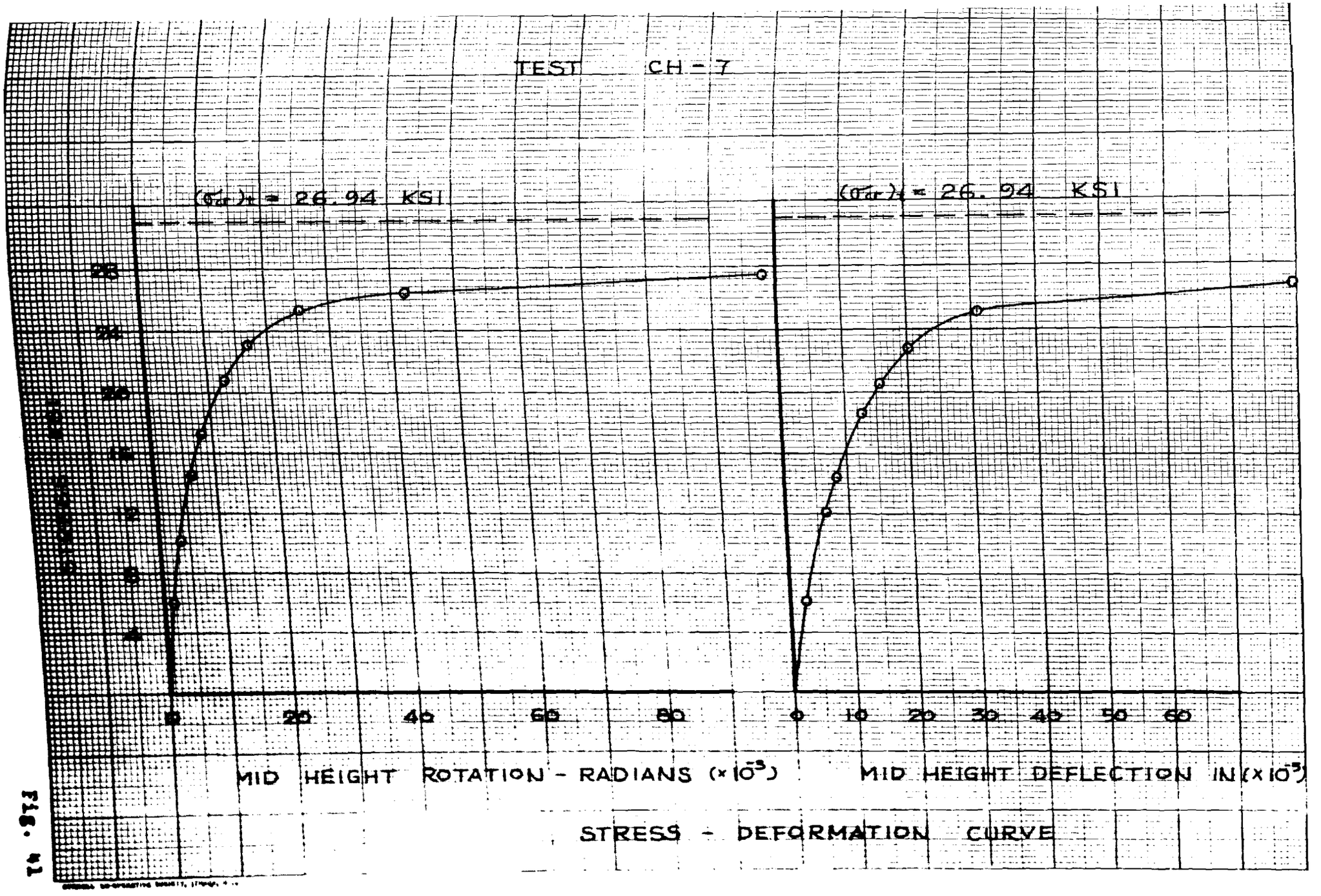

FIG. 41

STRESS - DEFORMATION CURVE

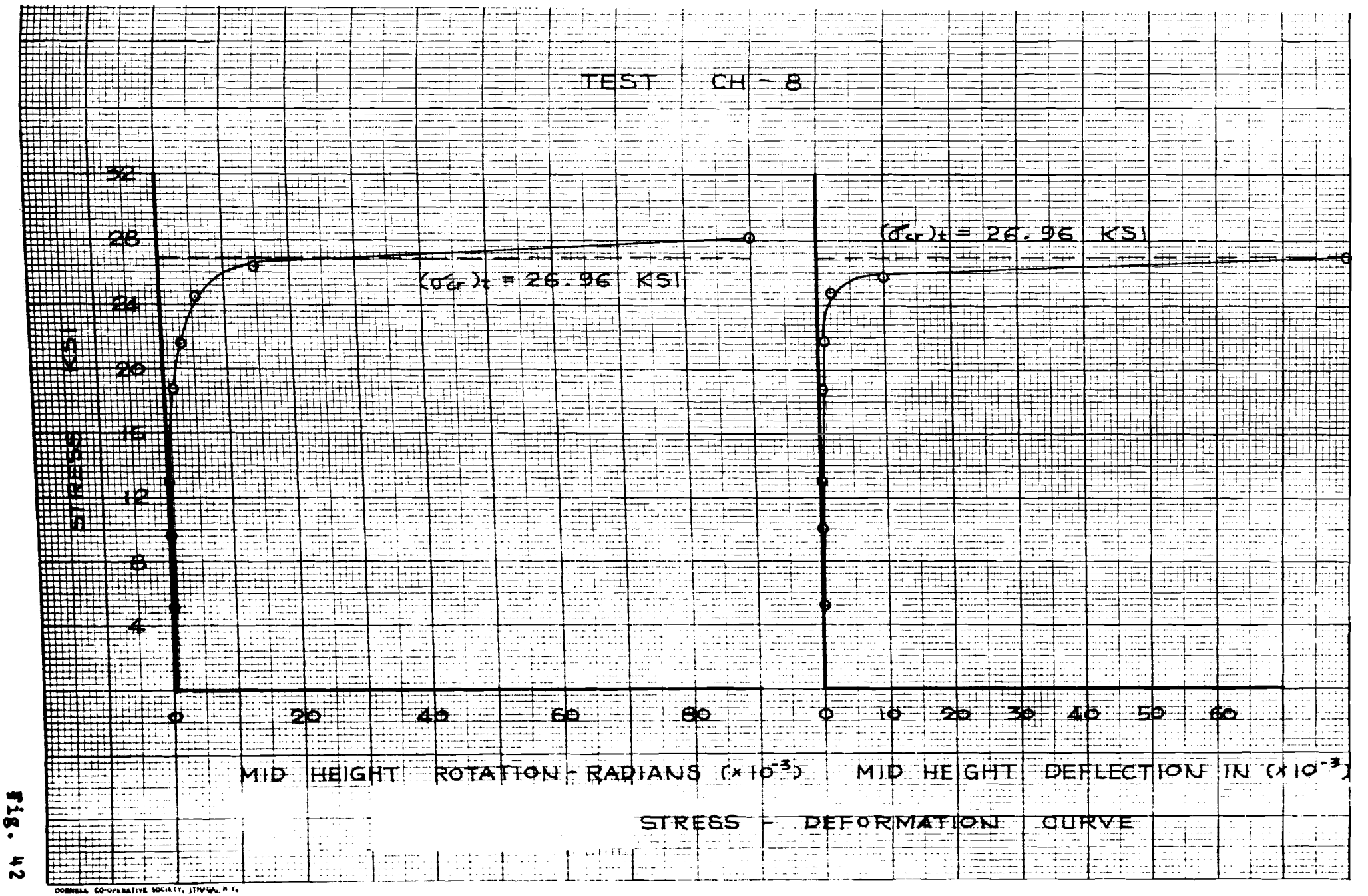
TEST CH - 8
32
28
24
20
16
12
8
4
σ_{cr} KSI
$(\sigma_{cr})_t$ = 26.96 KSI
$(\sigma_{cr})_t$ = 26.96 KSI
0
20
40
60
80
0
10
20
30
40
50
60
MID HEIGHT ROTATION - RADIANS ($\times 10^{-3}$)
MID HEIGHT DEFLECTION IN ($\times 10^{-3}$)
STRESS - DEFORMATION CURVE

Fig. 42

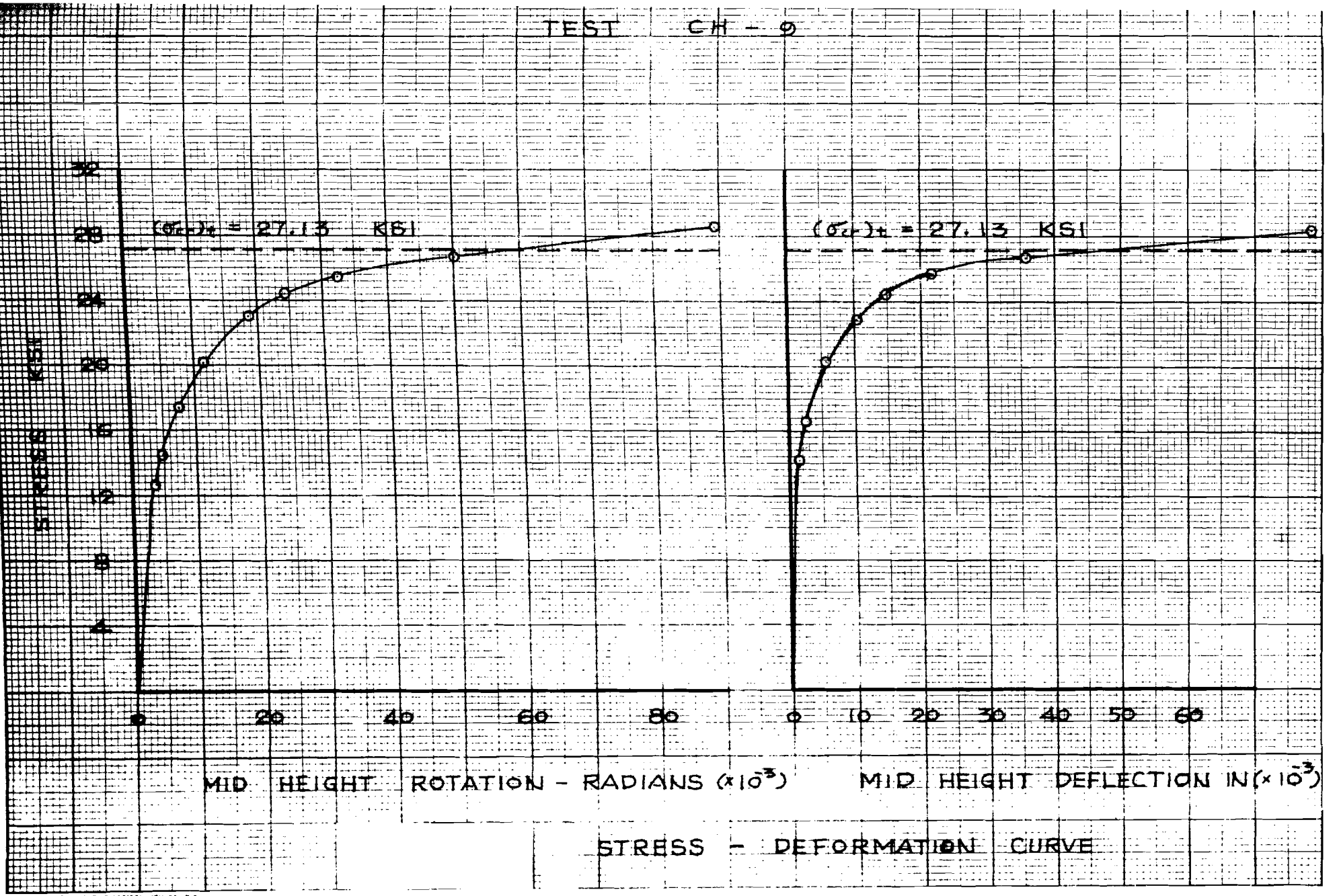

STRESS - DEFORMATION CURVE

Fig. 43

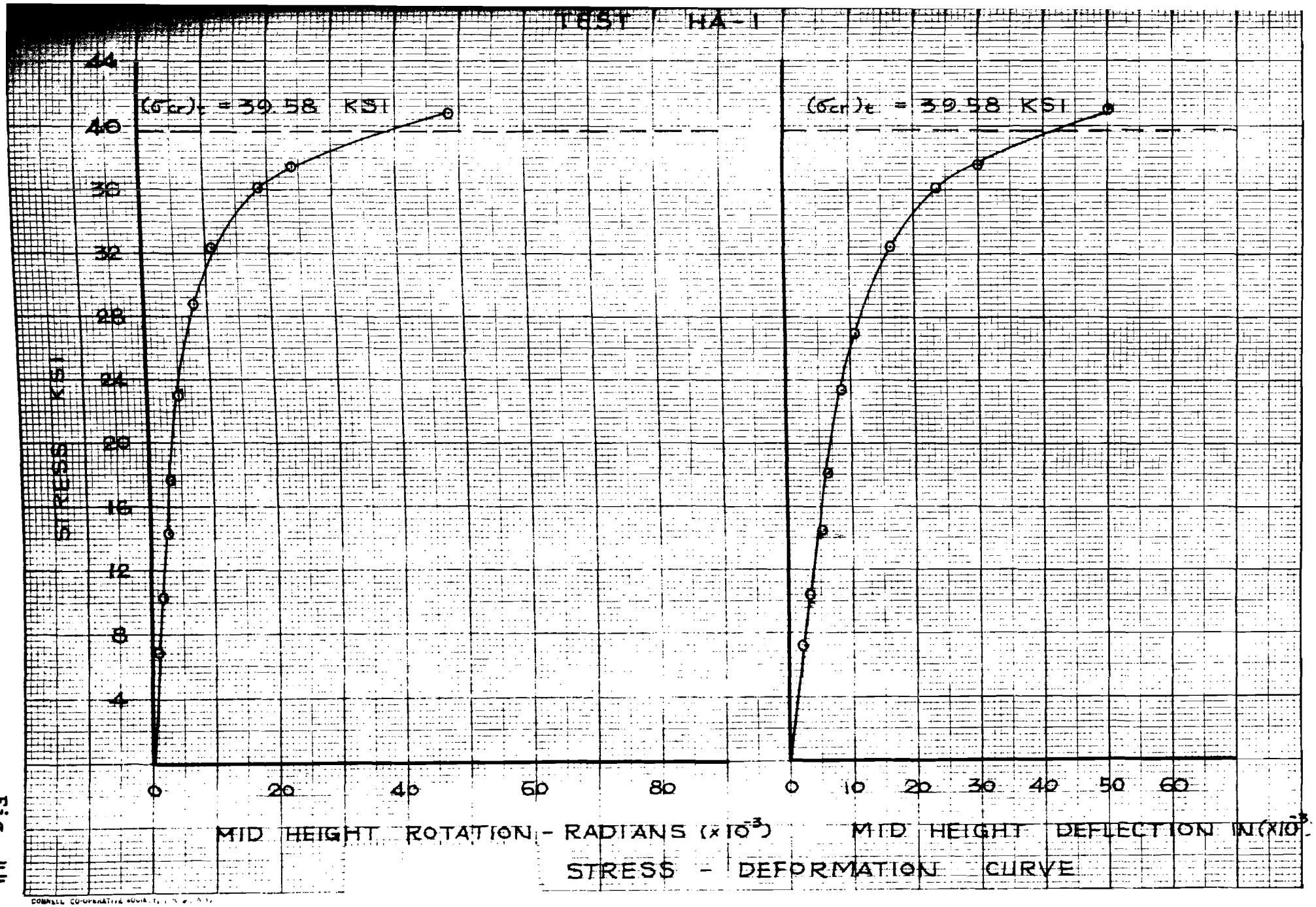

STRESS - DEFORMATION CURVE

Fig. 44

STRESS KSI
40
36
32
28
24
20
16
12
8
4
0
20
40
60
80
0
10
20
30
40
50
60
MID HEIGHT ROTATION - RADIANS (×10⁻³)
MID HEIGHT DEFLECTION IN (×10⁻³)
STRESS - DEFORMATION CURVE
(σzz)t = 38.19 KSI
(σzz)t = 38.19 KSI

Fig. 45

TEST HA-4
$(\sigma_r)_f$ = 28.0 KSI
$(\sigma_t)_f$ = 28.0 KSI
STRESS (KSI)
32
28
24
20
16
12
8
4
0
0
20
40
60
80
MID HEIGHT ROTATION - RADIANS ($\times 10^{-3}$)
0
10
20
30
40
50
60
70
MID HEIGHT DEFLECTION IN ($\times 10^{-3}$)
STRESS + DEFORMATION CURVE

Fig. 46

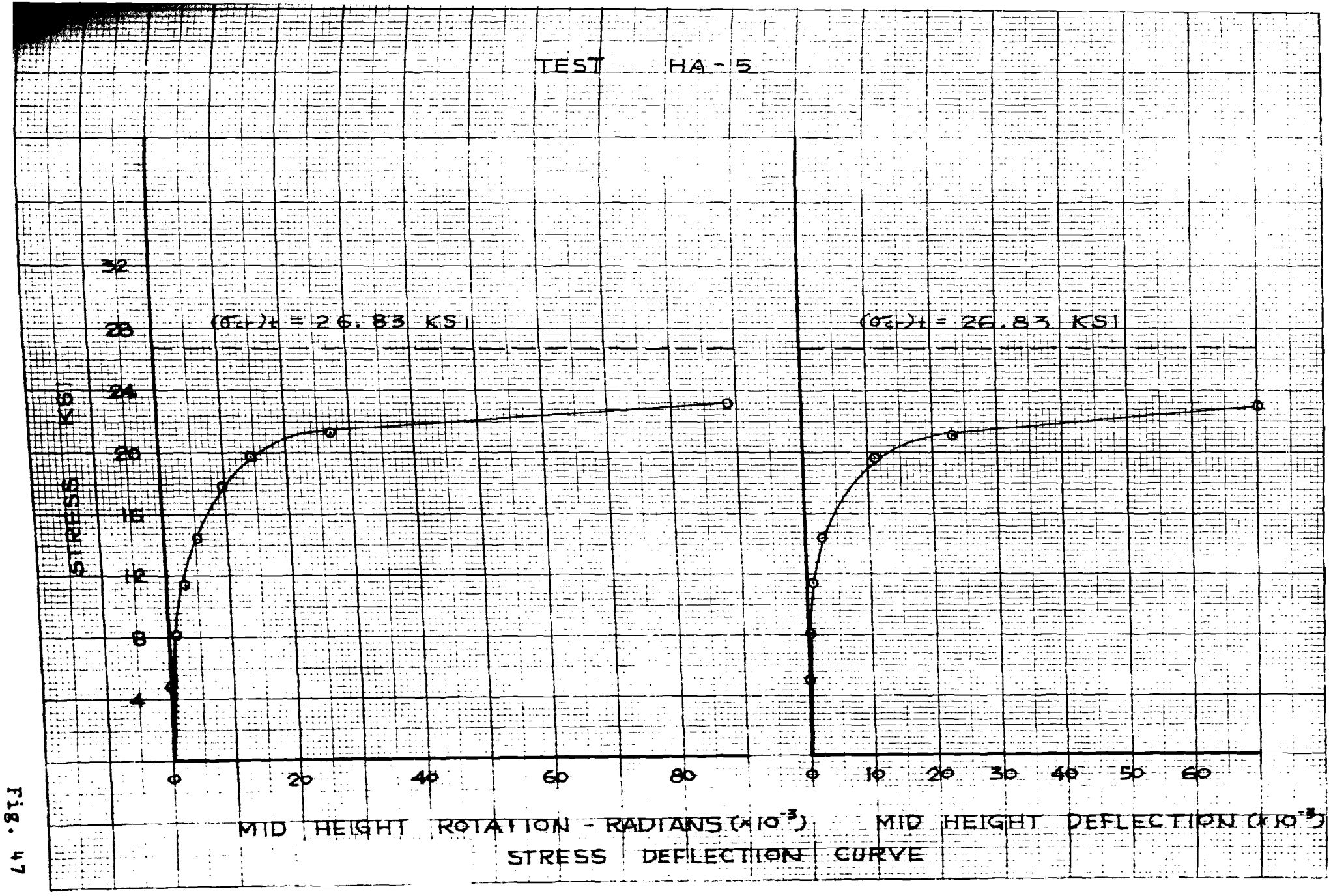
TEST HA-5
$(\sigma_{cr})_t$ = 26.83 KSI
$(\sigma_{cr})_t$ = 26.83 KSI
STRESS
32
28
24
20
16
12
8
4
0
20
40
60
80
0
10
20
30
40
50
60
MID HEIGHT ROTATION - RADIANS ($\times 10^{-3}$)
MID HEIGHT DEFLECTION ($\times 10^{-3}$)
STRESS DEFLECTION CURVE

Fig. 47

APPENDIX C

Torsional-Flexural Buckling Stress in the Inelastic Range on the Basis of "$G_t/G = \sqrt{E_t/E}$" Theory and Bijlaard's Effective Inelastic Shear Modulus Theory

TORSIONAL-FLEXURAL BUCKLING STRESS IN THE INELASTIC RANGE ON THE BASIS OF "$G_u\ G_t = \sqrt{E_t/E}$" THEORY AND BIJLAARD'S THEORY COMPUTED BY ITERATION METHOD

In order to compare the results based on the assumption stated in Eq. (7) of the main body of this report, computations are also made based on the more complicated expressions of G_t, i.e.,

$$\frac{G_t}{G} = \sqrt{\frac{E_t}{E}} \qquad \text{(D-1)}$$

$$G_t = E/[2 + 2\nu + 3(E/E_s - 1)] \qquad \text{(D-2)}$$

where E_s = the secant modulus,
the latter expression, (D-2), being Bijlaard's theory.

We shall start with Eq. (D-1). Assuming that the parabolic equation of E_t/E

$$\frac{E_t}{E} = 4.5\ \frac{\sigma}{\sigma_y}\left(1 - \frac{\sigma}{\sigma_y}\right) \qquad \text{(D-3)}$$

holds, the relationship is substituted into Eq. (D-1),, thus

$$G_t = G\sqrt{\frac{E_t}{E}}$$

$$= \frac{1.06E}{(1+\nu)}\sqrt{\frac{\sigma}{\sigma_y}\left(1 - \frac{\sigma}{\sigma_y}\right)} \qquad \text{(D-4)}$$

Then Eqs. (2) and (3) of the main body of this report become, respectively,

$$(\sigma_x)_t = \frac{4.5\pi^2 E}{(L/r_x)^2}\ \frac{\sigma}{\sigma_y}\left[1 - \frac{\sigma}{\sigma_y}\right] \qquad \text{(D-5)}$$

$$(\sigma_\phi)_t = \frac{1}{I_p}\left[\frac{1.06EJ}{(1+\nu)}\sqrt{\frac{\sigma}{\sigma_y}\left(1 - \frac{\sigma}{\sigma_y}\right)} + \frac{E_s C_w \pi^2}{L^2}\right] \qquad \text{(D-6)}$$

One sees that, upon substituting Eqs. (D-5) and (D-6) into

$$(\sigma_{cr})_t = \frac{1}{2K}\left[(\sigma_x)_t + (\sigma_\phi)_t - \sqrt{\{(\sigma_x) + (\sigma_\phi)_t\}^2 - 4K\,(\sigma_x)_t(\sigma_\phi)_t}\,\right], \qquad \text{(D-7)}$$

$(\sigma_{cr})_t$ is expressed implicitly as

$$(\sigma_{cr})_t = f[(\sigma_{cr})_t, E, \sigma_y, J, C_w] \qquad \text{(D-8)}$$

noting that at incipient buckling, $\sigma = (\sigma_{cr})_t$ in Eqs. (D-5) and (D-6).

The explicit expression of $(\sigma_{cr})_t$ would be in the form

$$(\sigma_{cr})_t^3 + f_2(\sigma_{cr})_t^2 + f_1(\sigma_{cr})_t + f_o = 0 \qquad \text{(D-9)}$$

where

$f_i = f_i$ (E, σ_y, dimensions of column)

The solution of Eq. (D-9) is very laborious. Fortunately, with the aid of an electronic computer, one can utilize an iteration technique to get a good approximate solution.

The procedure can be written in a form of flow chart for an electronic computer program as in Fig. (D-1). The variable, x, in the flow chart corresponds to $(\sigma_{cr})_t$ of the torsional-flexural buckling problem.

As to Bijlaard's theory, (D-2), the secant modulus, E_s, can be expressed by the use of Eq. (11) (see the Basic Theory) as follows:

$$E_s = \frac{(\sigma_{cr})_t}{\varepsilon} = \frac{4.5E(\sigma_{cr})_t}{\sigma_y\left[2.306 + \ln\left|\frac{(\sigma_{cr})_t/\sigma_y}{1 - (\sigma_{cr})_t/\sigma_y}\right|\right]} \qquad \text{(D-13)}$$

This expression is then substituted into (D-2) for G_t. The resulting equation for $(\sigma_{cr})_t$ by substitution of these moduli expressions into Eq. (4)(see the Basic Theory), is very complicated. However, the iteration method can also be applied to this case.

The computer results are listed in Table (D-1) together with the values computed by Eq. (15) for ready comparison.

It can be seen that the values computed from Eq. (15) are slightly lower than those from the other, presumably somewhat more rational theories. The differences, however, are small and of no practical consequence. Since Eq. (15) provides by far the simplest analytical tool, and since it leads to results satisfactorily confirmed by tests, its use, rather than that of one of the two other more involved expressions, appears justified.

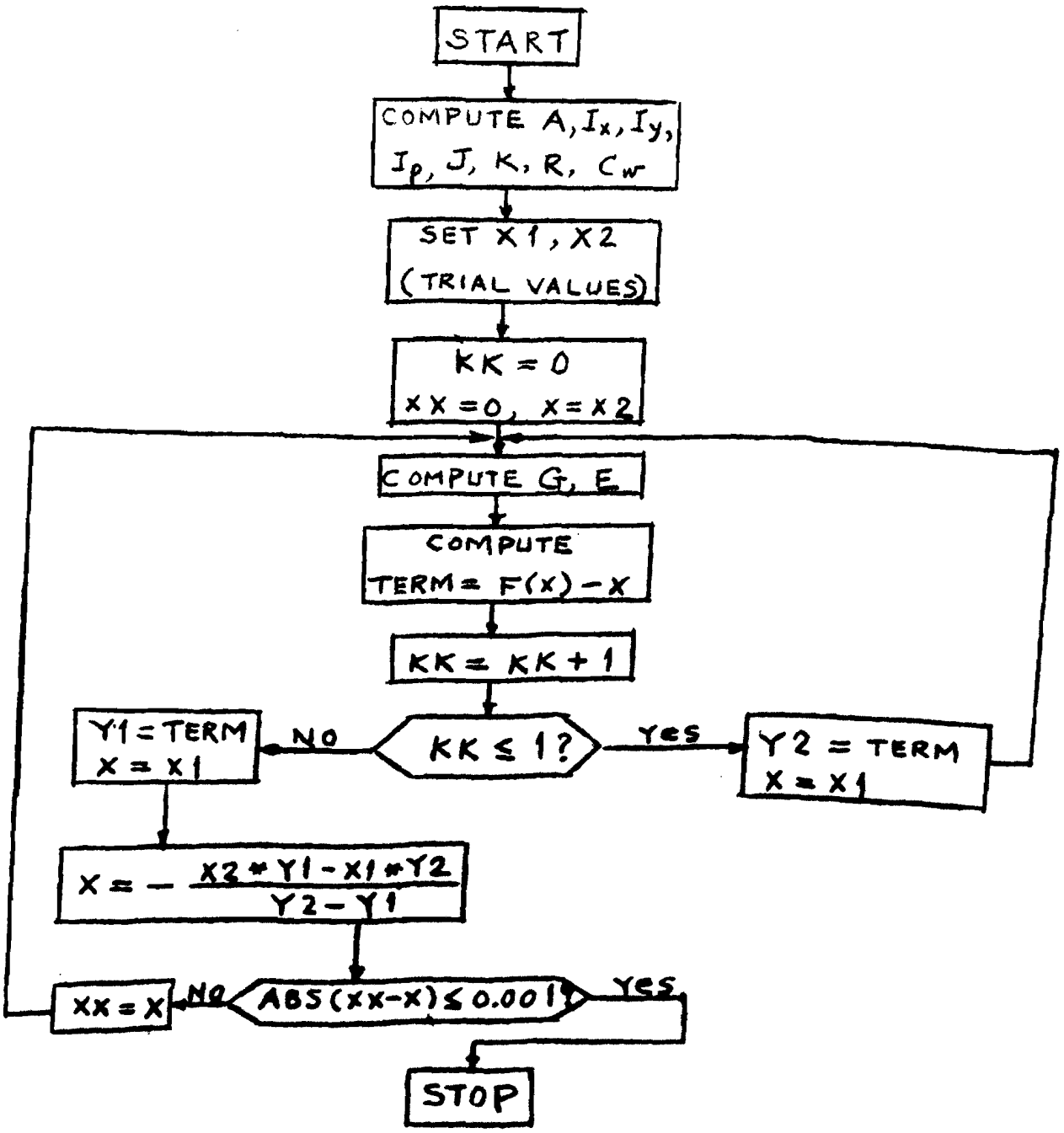

Fig. D-1 Flow Chart for the Iteration Method.

TABLE C - 1

Section	Specimen	$(\sigma_{cr})_t$ ksi		
		Eq. 15	Based on $G_t/G = \sqrt{E_t/E}$	Bijlaard
Plain Angle	A-1	35.87	37.08	39.43
	A-2	37.06	38.74	41.40
	A-3	30.80	31.07	33.18
	A-4	30.47	30.59	32.58
	A-5	28.85	28.27	29.61
Lipped Angle	LA-1	36.85	37.78	38.36
	LA-2	35.05	35.56	35.79
	LA-3	32.52	32.79	31.96
	LA-4	31.59	31.76	31.32
Channel	CH-1	37.48	38.33	38.53
	CH-2	27.91	28.31	28.68
	CH-3	27.06	27.53	27.93
	CH-4	24.05	24.49	24.70
	CH-5	24.89	25.19	25.38
	CH-6	25.79	26.16	26.44
	CH-7	25.45	25.97	26.34
	CH-8	25.74	26.12	26.40
	CH-9	25.80	26.19	26.46
Hat	HA-1	39.34	39.73	39.99
	HA-2	39.86	40.20	40.46